

Training toward Advanced 3D Seismic Methods for CO2 Monitoring, Verification, and Accounting

Type of Report: Progress

Frequency of Report: Quarterly

Reporting Period: October 1, 2011 – December 31, 2011

DOE Award Number: DE-FE002186 (UH budget G091836)

Submitting Organizations: Department of Earth and Atmospheric Sciences
Allied Geophysical Lab
University of Houston
Houston, Texas 77004-5505

Preparers: Prof. Christopher Liner – P.I.
Phone: (713) 743-9119
Fax: (713) 748-7906
Prof. Bernhard Bodmann (UH Math)
Dr. Jianjun Zeng (research scientist)
Dr. Martin Cassidy (research scientist)
Jintan Li (PhD candidate) ... coordinator for this report
Qiong Wu (PhD candidate)
Tim Brown (MS candidate)
Heather Yao (MS candidate)
Eric Swanson (non-thesis MS)
Heather King (non-thesis MS)
Johnny Seales (BSc candidate)

Distribution List:

FITS	FITS@netl.doe.gov	DOE-NETL
Chandra Nautiyal	Chandra.Nautiyal@netl.doe.gov	DOE-NETL
Vanessa Stepney	Vstepney@central.uh.edu	UH Contracts Office
Jack Casey	jfcasey@uh.edu	UH EAS Department Chair
Laura Bell	lbell4@uh.edu	UH EAS Department Admin
Lee Bell	lee.bell@geokinetics.com	Geokinetics (Industrial partner)
Keith Matthews	kmatthews@fairfield.com	Fairfield (Industrial partner)
Subhashis Mallick	smallick@uwyo.edu	Univ. of Wyoming
Steve Stribling	SStribling@gmocks.com	Grand Mesa Production

CONTENTS

Executive Summary	3
Geological modeling (June)	4
Fracture detection (Tim)	5
Flow simulation to seismic re-gridding (Jintan)	6
Multi-component processing (Qiong)	8
Update on first break picking algorithm (Heather Yao)	9
SEG meeting experience (Johnny)	9
Work plan for the next quarter	10
Cost and milestone status	11
Actual progress compared to milestones	11
Continuing personnel	11
Tables	13
Figures	15

Appendix A

Heather King, 2011, *Delineation of subtle geologic features by multi-attribute seismic analysis in Dickman field, Kansas, a potential site for CO₂ sequestration*

Appendix B

Eric Swanson, 2011, *Log property comparison to seismic amplitude analysis, Ness country, Kansas*

Executive Summary

This report presents major advances in progress made through the report period from October 1 of 2011 to January 31 of 2012 for the CO₂ sequestration training project in the Dickman field, Ness County, Kansas (Figure 1).

The method for topographic correction due to different datum elevations for the well and seismic corrections is implemented and discussed. A static time shift is necessary and is different from well to well by computing unique replacement velocity. The choice of velocity values is important and this step is mainly for the shallow sections.

Pre-stack seismic data has been mainly used to validate the preferentially oriented seismic anomalies related to paleo-stress effects. Velocity analysis in semblance panels is a standard tool used to identify the azimuthal anisotropic effects in the subsurface. Azimuthal AVO analysis is currently underway.

Re-gridding from flow simulator output to a seismic forward modeling grid is progressing. The choice of cell size is important to maintain subtle features in the complex geological structure at the carbon sequestration site, and the flow grid has to be downscaled to seismic resolution. A moving average smoothing method has been applied to the new property grid and tested to be useful. It provided a more reliable acoustic finite difference modeling result, to better identify CO₂ effects. Elastic modeling is currently underway.

Good progress has been made in multi-component data processing. Computer codes for trace population and horizontal rotation have been developed. Simulation is currently underway with more shots along the source line to provide enough CDP fold in order to analyze seismic velocities.

Geological modeling (June)

Work continues on the investigation and implementation of topographic corrections for well data as input to a stratigraphic-controlled velocity model. The importance, possible solutions and workflow steps were presented in the Quarter Q3 2011 report.

While tying well log data to the shallow section near the topographic surface in this area, the key step is to determine the vertical time shift of the well KB where the log reading depth is zero. The amount of the shift is different from well to well given the differences in elevation of KB and the seismic datum, ranging from 80-200 ft. The shift of well KBs, or the time shift of the floating datum elevation, is determined by the time shift calculated during the static correction of the seismic data.

During the static correction of seismic data, the floating datum elevation was corrected to the Seismic Reference Datum (SRD= 2600 ft above the sea level) by adding the static time shift, called *static time* (positive in downward direction). For all elevation values, the sign is therefore considered positive if below the mean sea level. In seismic-well ties of Dickman area, each well KB is always below the SRD time zero with a time-shift equal to the static time.

The static time shift is computed by the following equation using elevation differences between the floating datum and the SRD with a given replacement velocity (V_{rep}):

$$T_{stat} = 2 * (Z_{FD} - Z_{SRD}) / V_{rep}$$

In the Dickman Field, the Z_{FD} is the – (well KB), and the Z_{SRD} is -2600 ft (both are above mean SL therefore take positive signs). The replacement velocity represents the estimated average velocity of the seismic wave through the near surface medium (a mixture of water, air and near surface unconsolidated sediments). This velocity is supplied by the data processing company and, therefore, may not accurately represent the sonic velocity unconsolidated sediments. For instance, some processing companies use 2000 m/s to approximate the near surface velocity, most likely the sonic velocity through sea water and unconsolidated sea bottom sediments. For the mixture of air and unconsolidated sediments on land survey, the replacement velocity value theoretically should be no greater than this.

This replacement velocity applied by the processor must be known in order to do the computation for T_{stat} at each well KB precisely. This is not known, a trial-error test procedure can give general estimates of the time shift for well heads to tie the seismic profiles with acceptable precisions.

The elevation difference between the floating datum and the SRD in Dickman area ranges between 80 to 200 ft (30 - 60 meters). Assuming the $V_{rep} = 2000$ m/s as the possible upper limits of replacement velocity, the value range for the T_{stat} in Dickman area is between 30-60 ms ($2*30/2000$ to $2*60/2000$), as the lower upper and limits of time shift. This suggests that when tying well logs to the seismic profile, the position of each well KB should be shifted downward

by at least from 30 to 60 ms to correct the topographic effect and to restore the correct shapes of the tops for shallower formations. Based on this approximation, a new time-depth curve (or pseudo-checkshot curve) was created for each well, with the first time-depth pair at the KB elevation. The curve was assigned as the default T-D curve for seismic-well tie above the first well-defined time-depth pairs on a stratigraphic formation top (Stone-Corral) for wells with logs starting above the formation top. These wells were used as correction points to adjust the amount of time shift. From well log analysis, the Stone Corral is a 40 feet thick anhydrite-bearing red bed with very low gamma (10-25 API) and high velocity (13500 ft/s). In seismic data, this horizon is a sharp trough around 420-430 ms. The newly added time pairs were used as velocity correction points to help adjust the time shift for most wells with log measurements starting below the Stone Corral Formation.

The well-defined Stone Corral Formation was also used as surface velocity input (layer-averaged velocity from Stone Corral to Heebner Shale). Graphic display of the corrections and velocity model for the shallow sections will be included in the next report.

Previous models focused on the deep section using the Fort Scott limestone as reference datum, more than 4200 feet below the floating datum and SRD. Therefore topographic time shifts were minor and errors did not significantly affect the time-depth conversion or interpretation.

Fracture detection (Tim)

Work proceeds towards characterizing sub-resolution fracturing in the Mississippian reservoir that is related to Pre-Pennsylvanian tectonic deformation. In previous reports we showed, narrowband-filtering at low frequencies shows preferentially oriented seismic anomalies that are potentially related to these paleo-stress effects (Figure 2). We continue to examine the validity of these features by analyzing pre-stack seismic data (p-wave only) and digital well logs. The results will be used to test the hypothesis that low frequency seismic features indicate natural fractures, and therefore give information on reservoir and seal structural integrity. This section of the report will focus on the pre-stack seismic analysis.

The first step in the pre-stack seismic analysis method is to find any dependence of velocity on azimuth, or azimuthal anisotropy. Preferentially oriented sub-vertical fracturing will produce azimuthal anisotropy and the effects should ideally be present in the pre-stack data. The procedure for detecting azimuthal anisotropy is as followed: 1) sort the data into common mid-point (CMP) bins, 2) sector the data based on azimuth, and 3) perform velocity analysis on these azimuthal gathers, specifically from sub-reservoir reflectors. Results will only show anisotropic effects, if any, in the overburden because the method considers the response from the wave field above the reflector. Since the last major tectonic episode only affected Pre-Pennsylvanian rocks, any azimuthal anisotropic effects should be constrained to units below the Mississippian-Pennsylvanian unconformity. This hypothesis is also being tested.

The low-frequency anomalies have orientations close to that of NW and NE, as indicated by Figure 2. Regional studies show that fluid-flow in the reservoir favors the NW-SE direction. Therefore, fractures with this orientation are presumed to be open while orthogonal sets are considered healed.

Our pre-stack seismic data makes up approximately a fifth of the entire survey and only covers the southern portion of Dickman field. This limitation reduces the fold severely and leads to sparse azimuthal-offset coverage. Figure 3 shows the offset vs. azimuth from a 500 ft X 500 ft CMP bin. For a given azimuth, obvious gaps in the offset can be seen. Therefore, gathers are azimuthally sectored by 5-10 degree increments in order to fill-in these offset gaps.

Figure 4 shows azimuthally sectored (10°) CMP gathers that approximate these directions. Here, the Mississippian-Pennsylvanian unconformity is approximated at a time of 848 ms in the Dickman survey. A robust reflector at 875 ms, near-offset, represents the Viola formation and serves as an optimal event for NMO velocity comparison between gathers.

Figure 5 shows stacking-velocity semblance plots for the corresponding azimuthal gathers. Based on the geometry of the open fracture sets, the fast velocity direction (V_{fast}) and the slow velocity direction (V_{slow}) should be in the NW-SE and the NE-SW directions respectively. However, results show a severe similarity in stacking velocity profiles, especially at 875 ms (Viola formation). This lack of velocity discrepancy does not deny the presence of fracturing in the reservoir. The major pitfall with this method is the lack of resolution being considered. As mentioned, this velocity analysis only classifies the azimuthal anisotropic effects from the overburden, which may be weak considering the reservoir architecture and therefore not detectable by this method.

To improve resolution, future work will focus on azimuthal AVO analysis, which considers the change in reflection properties as a function of azimuth for a given reflector. Also, fuzzy inference systems will be used to detect fracture indicators from conventional well logs in order to provide some ground-truth information on reservoir structure.

Flow simulation to seismic re-gridding (Jintan)

Re-gridding flow simulator output to a seismic forward modeling grid presents difficulties. A flow simulation model typically is composed of grid blocks that are much larger laterally than 3D seismic bins, yet in the vertical direction the blocks are very thin, far below seismic resolution limits. Thus flow-to-seismic re-gridding includes both lateral downscaling and vertical upscaling.

In the Dickman Field, for example, the flow simulation model is built of blocks 500 ft x 500 ft in the x-y plane and variable thickness over the depth interval 2750-5000 ft. The investigated CO₂ sequestration target (uppermost Miss carbonate and basal Penn sands) is about 80 ft thick. Reservoir properties in each flow simulator block are associated with a (potentially) different block thickness, in fact some block properties may be missing due to presence of an unconformity surface. In addition to missing section, there is also the problem of very thin simulation layers

that are typically built from well log data that has a much higher vertical resolution than seismic data.

For example, consider a simulation model with two vertically-adjacent points 10 ft apart. If a 5ft seismic grid spacing is chosen, then the properties at the middle point will be unknown, and require interpolation. If the two simulation model points are 2 ft apart, then they must be somehow averaged up to the 5 ft seismic grid spacing.

In our model, the spacing of points in z direction varies from 0.5ft to 100ft. The choice of spacing can be tricky if it has to accommodate all the circumstances that were discussed. If the unknown/missing points cannot be resolved correctly, they may produce sharp edges which will greatly affect the velocity model, and have to be fixed. There are many interpolation methods that can be applied to this case, such as piecewise linear, and cubic spline interpolation, or averaging, but they seem to be a little redundant. The easiest method is to set the vertical grid spacing as small as possible, say the smallest spacing between two adjacent vertical points, then it can include all the subtle features that have been embedded in the cells. After this step is done, the intermediate points between the large spacing points will be filled up with the same values as the above one. The data points have been assigned values, but it may still have some sharp boundaries due to this estimation. So a smoothing method is applied to reduce the sharp edges.

The smoothing method I used is to smooth data using a 5-point moving average, and is only applied to the calculated velocity model. The difference before and after smoothing can be seen in Figure 6a and 6b. It avoids the sharp boundary that's caused by the estimation from the neighboring values, and is ready for a more reasonable seismic forward modeling result.

A leakage scenario has been tested in Figure 7. The leakage is set at the surface by assigning a fault across the flow simulation model. This is to test how CO₂ has leaked and its flow path through the seal. The saturation at year 2250 is illustrated in Figure 8. The velocity difference is strongly correlated to the saturation change, and is plotted in Figure 9. The 2D acoustic forward modeling results via plane wave at the 1st year of injection and last year of monitoring are influenced by the velocity difference at the surface. The results show both the time shift and amplitude change (Figure 10).

In summary, the regridding problem can be summarized as follows. The flow grid (FG) is regular in x-y and irregular in z, meaning that all grid blocks have the same x-y size but variable thickness. The desired seismic grid (SG) is regular in x-y-z. Let us call the grid node intervals in each direction dx, dy and dz. The flow grid (dx,dy) is much larger than the seismic grid (dx,dy), this requires downscaling of the flow grid to the seismic grid interval. In the vertical direction things are more complicated. The irregular flow grid dz can range from zero (unconformity) to something on the order of 100 ft, while the seismic grid is desired to be regular and something like 5-10 ft. Depending on the thickness of each individual block, this may require upscaling or downscaling, and missing section must be addressed carefully since every point in an earth model for seismic simulation must contain parameter values.

Multi-component processing (Qiong)

Our short-term goal of this project is now to establish a data volume of simulated elastic multi-component prestack data, sort to CDP gathers and analyze velocity P and S-waves. Progress on seismic simulation and processing in last quarter could be summarized by the flow chart in Figures 11 and 12. We simplify the input parameters to establish a demo. For testing, we have used a Vp-Vs ratio of 2, held density constant, and generated 6 seconds of data (2 ms sampling, 3000 time samples). Elastic simulation with the Anivec reflectivity modeling program generates radial, transversal and vertical response components (Figure 13). The multi-component data is input to a Matlab program we developed that performs geometry and horizontal rotation based on Geokinetics' 3D survey design (Figure 14). The output are seismic response X, Y, Z components in binary format (Figure 15a, 15b, 15c). We also set header words such as source coordinate, receiver coordinate, azimuth and offset.

SegyMat is an open source MatLab software for reading and writing SEG-Y formatted files. We resort to SegyMat to add header words to corresponding seismic data subsequently (3 component * 3547 traces * 21 shots), so that SEG-Y formatted X, Y, Z component were obtained. To enable processing these data in Seismic Unix, a shell script is written to strip SEG-Y headers and output SU formatted data. Non-zero header words in an SU file are shown below (2050 is shot number):

```
suedit < x_csg2050.su & % SU header of shot 2050 X component
3547 traces in input file
  tracr=3547 tracf=3547 offset=14944  sx=1565586 sy=694372 gx=1575903
  gy=705183 ns=3000 dt=2000 year=2011 day=314 hour=1
  minute=50 sec=4
```

```
suedit < y_csg2050.su & % SU header of Y component.
3547 traces in input file
  tracr=3547 tracf=3547 offset=14944 sx=1565586 sy=694372 gx=1575903
  gy=705183 ns=3000 dt=2000 year=2011 day=314 hour=1
  minute=50 sec=28
```

To sort and calculate Common Mid Point (CMP), another shell script was developed to concatenate X, Y and Z component common shot gathers of all 21 shot together subsequently (Figure 16). Header words of the X component are listed below:

```
suedit < x_csg_21.su & % x_csg_21.su is file name
69872 traces in input file
  tracr=2479 tracf=2479 offset=6950 sx=1567703 sy=696435 gx=1574488
  gy=697941 ns=3000 dt=2000 year=2011 day=314 hour=2
  minute=14 sec=15
```

CMP gathers were sorted for each of 21 simulated shots. In Figure 17 CDP geometry of shot 1, shot 10 and shot 19 are plotted together, and dimension of CDP grid is 330 * 55 ft (55 ft along receiver line, 330 ft in perpendicular which agree to the number in the project proposal); CDP point in green box is zoomed in and shows in Figure 18. In Figure 18 we observe that most of the CDP points of shot 1 and shot 19 share the same location and fold. Scrutinizing CDP points of all shots, we found CDP points fold up in every 18 shots. Then 21 shots are not enough to give us

enough CDP fold, therefore, next step is to generate simulated shot at an interval of 18 shots along source line. After getting enough fold we can sort CDP gather and proceed to velocity analysis.

Update on first break picking algorithm (Heather Yao)

The *suaglpickr* is a program in Seismic Unix (SU) to pick the first arrival time for multiple traces and calculate both the mean time and standard deviation for the time. It has been validated and shown to be efficient and reliable. Therefore, we used *suaglpickr* on physical modeling data to find travel times in various experiments.

The experiments were conducted in the Allied Geophysical Lab (AGL) and Rock Physics Lab (RPL). Two aluminum samples of different size were used in the experiments for comparison. Two different transducers were tested source and receivers, an AGL 3-component transducer and an RPL transducer. The experiments measured acoustic response to determine first arrival time through test samples, and with the transducers in direct contrast (to establish zero-time).

Figures 19, 20, and 21 show results from processing data from AGL using *suaglpickr*. Tables 1, 2 and 3 show test results for P wave velocity in two acquisition systems (RPL and AGL), with two transducers. Two calibration samples were tested through two different samples: AGL sample (KONG) and RPL sample. Table 4 shows the comparison for all the velocities with different components. The data with 3-C transducer in RPL system is chosen to be the reference data for future use.

SEG meeting experience (Johnny)

SEG 2011, located in San Antonio, TX, was quite an experience for me seeing it was my first attendance of a major conference. There were many people to meet and great exhibits to visit, and presentations to attend. From an undergraduate perspective, it was an unprecedented look into opportunities the energy industry has to offer while still maintaining a qualified learning environment.

Preparing for the event was quite of process of revision and preparation for what was not only my first abstract, but also first oral presentation. During the weeks leading to the conference, the CO2 group members assisted in not only the quality control for the content of my presentation, but also in the visual appeal of the slides in an effort to compose my figures in as professional a way as possible. There were numerous attempts to rehearse my presentation in its entirety with the presence of a knowledgeable audience that could not only ask questions in the end, but help brainstorm ideas in ways to present and clarify obscure ideas. With the aforementioned assistance, the stress related to preparing for such a presentation was significantly reduced.

The guidelines provided for speakers at the event were not only well thought out, but also beneficial in maintaining order and lowering stress leading up to the presentation. The process of loading and editing a presentation was simplified to meeting in a room and loading the file onto a server that would later be loaded to the computer at your room. The morning of my talk, I was able to attend an informative breakfast that not only was delicious, but also provided a thorough understanding of how the procedures for the talk would be administered.

When it was time for my presentation, I arrived at the beginning of my session to a room, which I had already scouted out. I knew what the layout of the room and audience was. When it was my turn, I had already seen two presentations performed. One unlucky factor I had was the presenter in front of my elapsed his full allotted time. This threw me off a little and began my presentation on a down note. I then realized that many people were leaving the room which again rattled my attention a little. As I began my presentation, I attempted to speak as clearly as possible. I feel I stumbled a few times and made a few mistakes as well as ended a little short, but I did not have too many questions.

After reflecting on my presentation, I definitely have room for improvement. I should have slowed my sentences and gone into further depth with each slide. On the other hand, I feel I learned quite a lot from this experience. I was one of few undergraduates speaking, and this tells me it is quite an accomplishment to achieve what I have. I will take the constructive criticism I have received from my peers and professors in regards to the build- up of and completion of the presentation process to better myself for the next time I undertake such an endeavor.

Work plan for the next quarter

June: will finish the work on shallow layer model which includes the corrected velocity model, log-well tie, depth-conversion for the attribute volumes, all for shallow layer. A new draft will be written for the structural interpretation using attributes for **AAPG** April 2012, which will include results for the shallower layers.

Tim: future work will focus on azimuthal AVO analysis, which considers the change in reflection properties as a function of azimuth for a given reflector. Also, fuzzy inference systems (FIS) will be used to detect fracture indicators from conventional well logs in order to provide some ground-truth information on reservoir structure.

Jintan: will continue working on resolving the scaling issues from flow simulation output to seismic modeling, and focus on analysis of amplitude changes and time shift due to CO₂ injection. A more reliable elastic forward modeling package is needed to obtain accurate results for comparison.

Qiong: will generate simulated shot at an interval of 18 shots along source line till getting enough fold, then sort CDP gather and analysis velocity in X, Y, Z three directions to study velocity of P wave and S wave.

Heather Yao: will finish up the master thesis and defense by the end of Spring semester; and lab work transaction with Jiannan Wang (a new PhD student advised by Dr. Liner)

Cost and milestone status

Baseline Costs Compared to Actual Incurred Costs

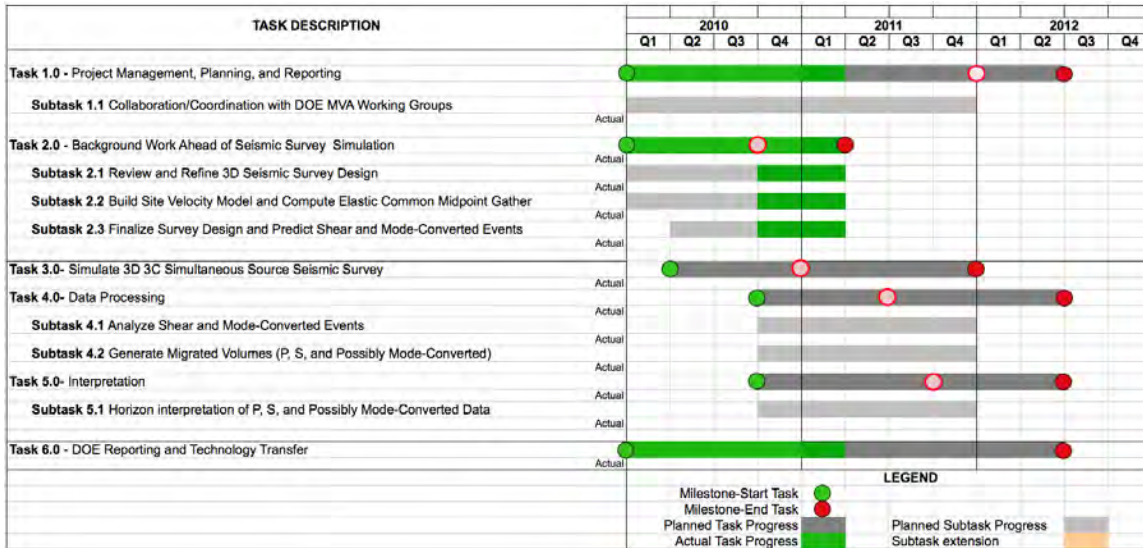
7/1/11 – 9/30/11	Plan	Costs	Difference
Federal	\$36,668	\$23,415	\$13,253
Non-Federal	\$4,063	\$0	\$4,063
Total	\$40,730	\$23,415	\$17,316

Forecasted cash needs Vs. actual incurred costs

Notes:

- (1) Federal plan amount based on award of \$293,342 averaged over 8 reporting quarters.
- (2) Non-Federal plan amount based on cost share of \$32,500 averaged as above.
- (3) Cost this period reflects salary for J. Zeng (3 mo).

Actual progress compared to milestones



Continuing personnel

Prof. Christopher Liner is Principle Investigator and lead geophysicist. He is a member of the SEG CO₂ Committee, Associate Chairman of the Department of Earth and Atmospheric Sciences, Associate Director of the Allied Geophysical Lab, and has been selected to deliver the 2012 SEG Distinguished Instructor Short Course.

Prof. Bernhard Bodmann is co-PI for the Geokinetics project and a member of the University of Houston Mathematics Department.

Dr. Jianjun (June) Zeng has been working exclusively on this project since Dec 2007 and is lead geologist.

Dr. Martin Cassidy is a research scientist in the Department of Earth and Atmospheric Sciences at the University of Houston.

Ms. Jintan Li is a 3rd year PhD student in geophysics who joined the project in Aug 2009. She is funded by Allied Geophysical lab at this time. Her thesis will be time-lapse seismic modeling (4D) for conducting dynamic reservoir characterization of the Dickman Field.

Ms. Qiong Wu is a 3rd year graduate PhD student in geophysics who joined the project in January 2010 as a research assistant. She will be funded year-round out of the project.

Mr. Tim Brown is a 2nd year MS student in geophysics.

Ms. Heather Yao is a 2nd year MS student in geophysics.

Tables

AGL system, 3-C transducers, 1mhz, P wave measurements for velocity in RPL Sample and Kong

Direct Contact Time (s)	Sample Time without Correction Kong(s)	Travel Time (with Correction) Kong(s)	Sample Time without Correction RPL Sample (s)	Travel Time (with Correction) RPL Sample (s)
0.0067	0.1657	0.159	0.1269	0.1202
Std_dev		0.001203		0.00028
Sample Length	101.33mm	0.00001m (error of scalar)	76.20mm	0.00001m (error of scalar)
Velocity	6373m/s	49m/s	6339m/s	13m/s

Table1: AGL system, 3-C transducers, 1mhz results for P wave velocities for two samples

RPL system, 3-C transducers, 1mhz, P wave measurements for velocity in RPL Sample and Kong

Direct Contact Time (s)	Sample Time without Correction Kong(s)	Travel Time (with Correction) Kong(s)	Sample Time without Correction RPL Sample (s)	Travel Time (with Correction) RPL Sample (s)
0.000792	0.159984	0.159192	0.120736	0.119944
Std_dev		0		0
Sample Length	101.33mm	0.00001m (error of scalar)	76.20mm	0.00001m (error of scalar)
Velocity	6365m/s	0.6m/s	6353m/s	0.6m/s

Table 2. RPL system, 3-C transducers, 1mhz results for P wave velocities for two samples

RPL system, RPL transducers, 1 mhz, P wave measurements for velocity in RPL Sample and Kong

Direct Contact Time (s)	Sample Time without Correction Kong(s)	Travel Time (with Correction) Kong(s)	Sample Time without Correction RPL Sample (s)	Travel Time (with Correction) RPL Sample (s)
0.000072	0.160204	0.160132	0.120076	0.120004
Std_dev		0		0
Sample Length	101.33mm	0.00001m (error of scalar)	76.20mm	0.00001m (error of scalar)
Velocity	6328m/s	0.6m/s	6350m/s	0.6m/s

Table 3. RPL system, RPL transducers, 1mhz results for P wave velocities for two samples

	3C-Tansducer AGL System 20 traces	3C-Trasnducer RPL System 1 trace (REFERENCE)	RPL-Transducer RPL System 1 trace
P wave velocity in KONG m/s	6373 Error: 49 +0.126%	6365	6328 -0.581%
P wave velocity in RPL Sample m/s	6339 Error: 13 -0.220%	6353	6359 +0.094%

Table 4. Comparison for velocities with different components.

Figures

Dickman Field Site

- 3D Seismic
 - 3.325 sq.mi.
- 142 wells
 - 54 in 3D area
 - 45 with digital logs
 - GR (43), Resistivity (25),
 - Neutron (27),
 - P-Sonic (6), Density (3)
 - 7 with core
 - porosity and permeability
 - 3 full deep saline aquifer penetration

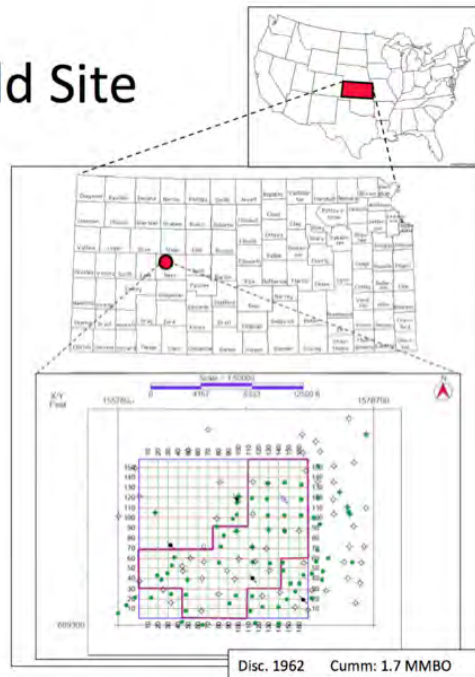


Figure 1. Area map depicting the location of the project area, Dickman field, Ness County, Kansas. On detail map, live 3D seismic area is shown as purple polygon.

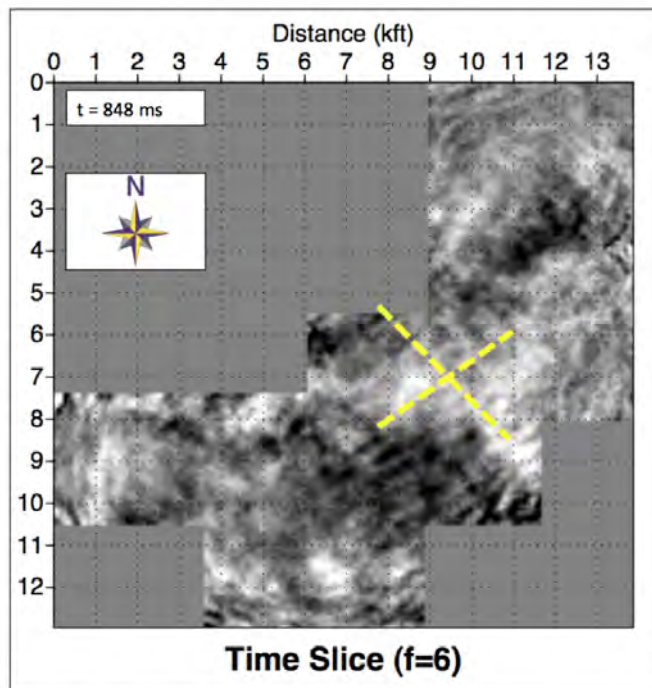


Figure 2. 6 Hz slice at 848 ms showing NE-NW trending features that are potentially related to fracture networks. Yellow dashed lines represent the respective orientations.

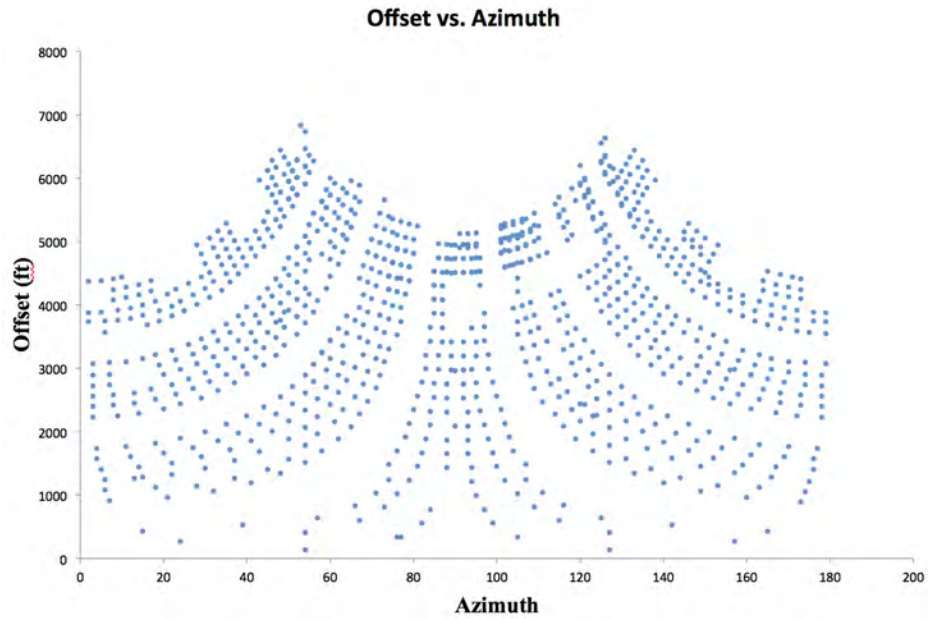


Figure 3. Offset vs. azimuth plot for a 500ft by 500ft CMP bin. Notice the frequent gaps is offset for a given azimuth.

Figure 4a. 10° azimuthal sectoried CMP gather from 500ft by 500ft bin centered on 50°. Prominent reflection events are indicated by the red arrows. Times are muted for an offset depth-ratios that exceeds unity. Notice that the gathers still contain sparse offset coverage.

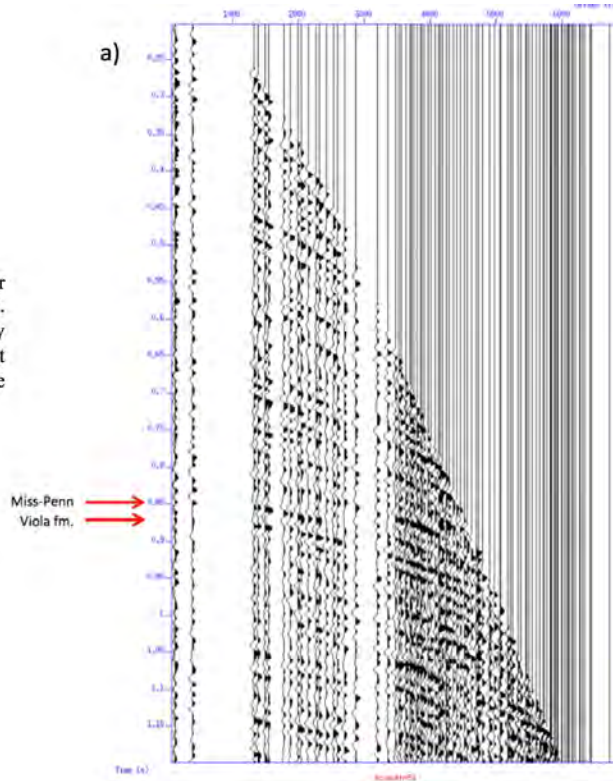


Figure 4b. 10° azimuthal sectored CMP gather from 500ft by 500ft bin centered on 131°.

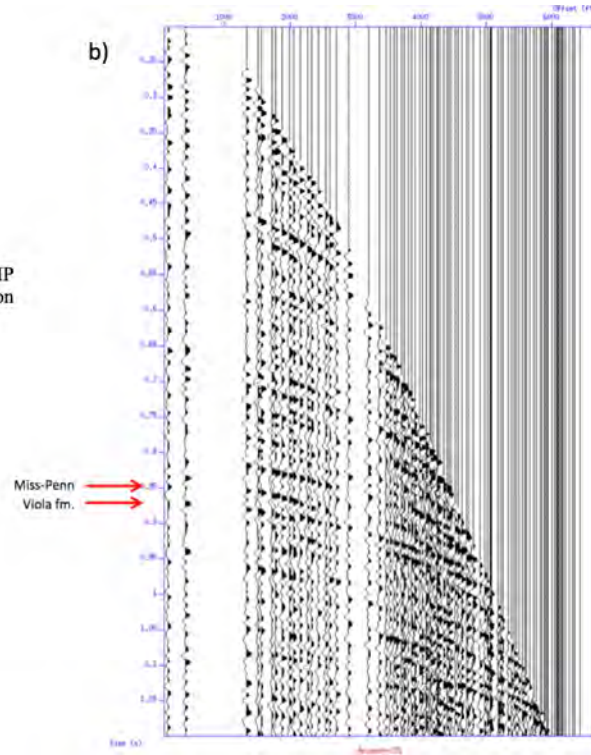
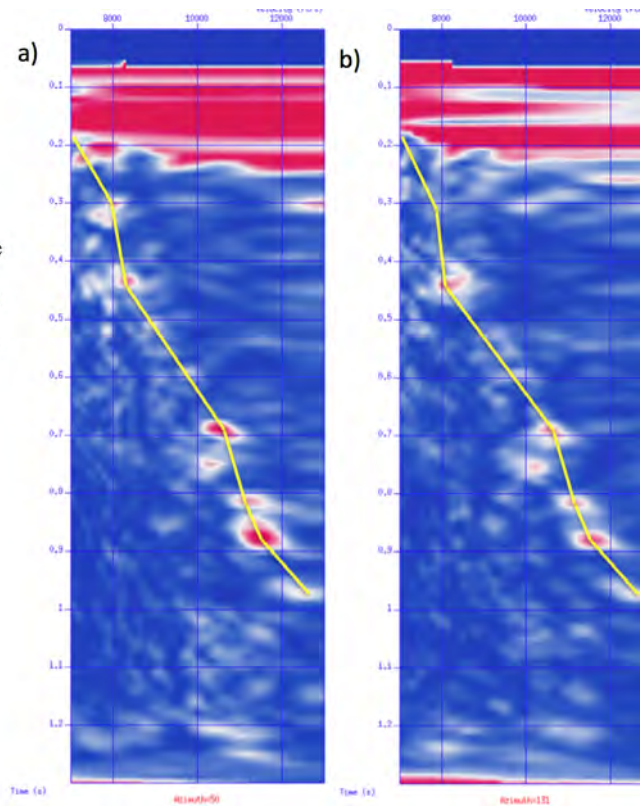


Figure 5. Stacking-velocity semblance plots for corresponding azimuthally sectored CMP gathers: (a) 50° and (b) 131°. Both stacking velocity profiles show similar trends, especially at 875 ms (Viola fm.) where the velocity is approximately 11500 ft/s.



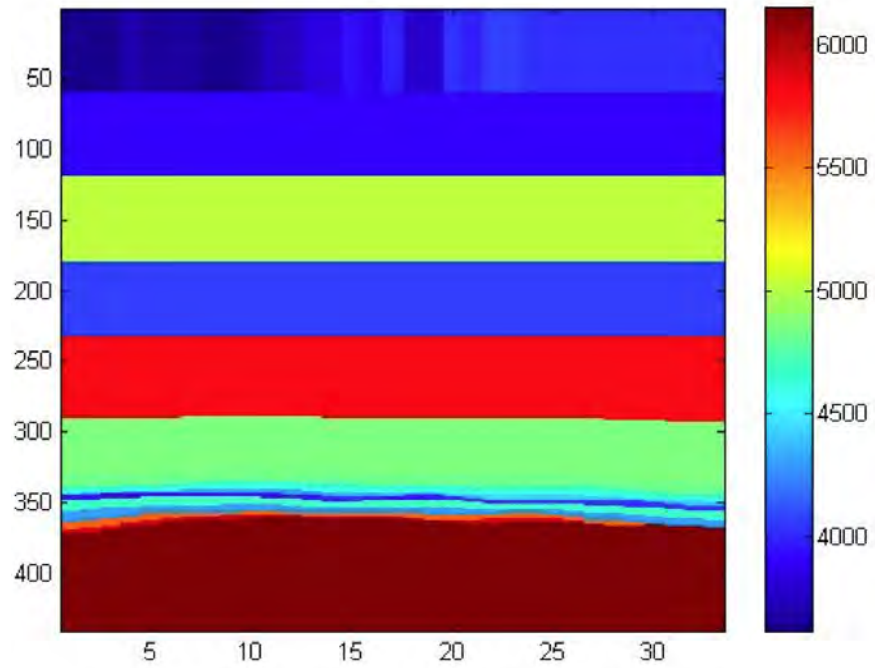


Figure 6a: Velocity model for year 2000' without smoothing applied

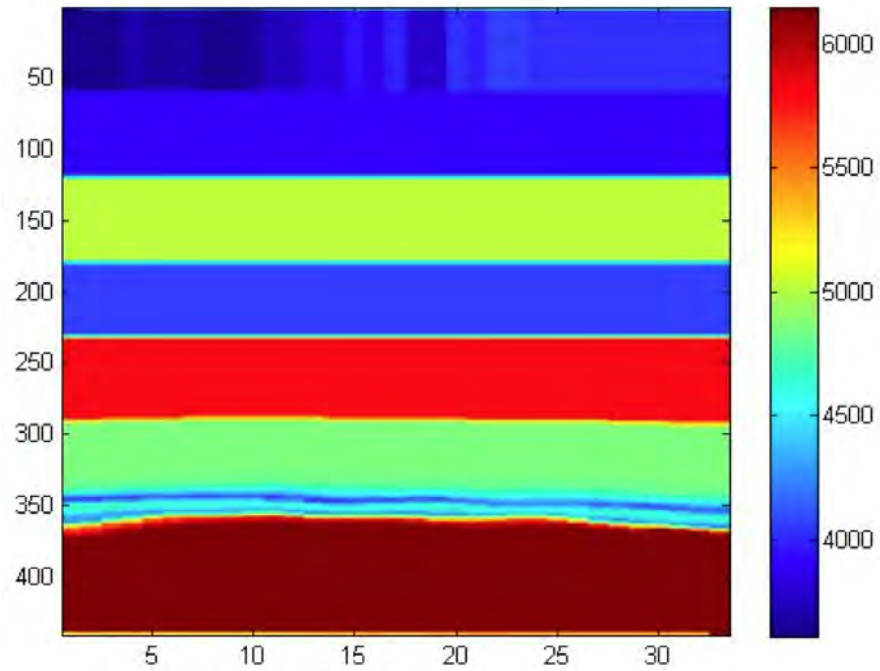


Figure 6b : Velocity model for year 2000' with smoothing applied

Gas Saturation at 250 years

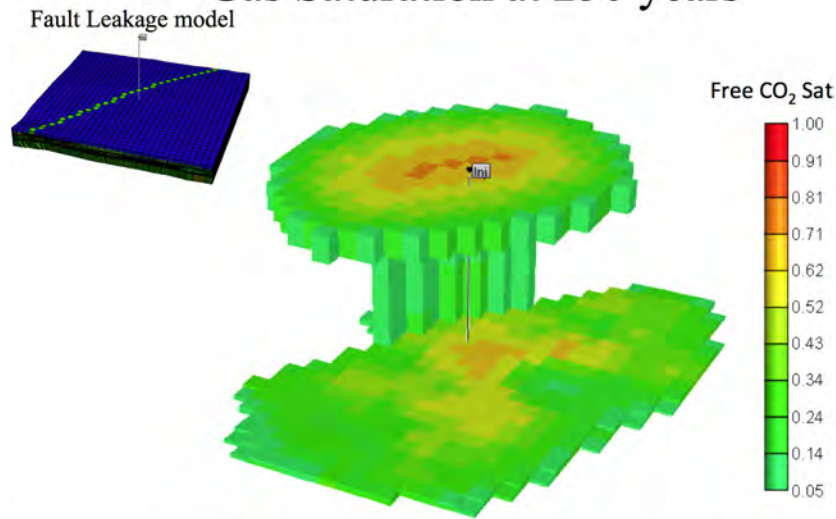


Figure 7 : Fault leakage model with CO₂ leakage to the surface after 250 years injection (after Geng, 2011).

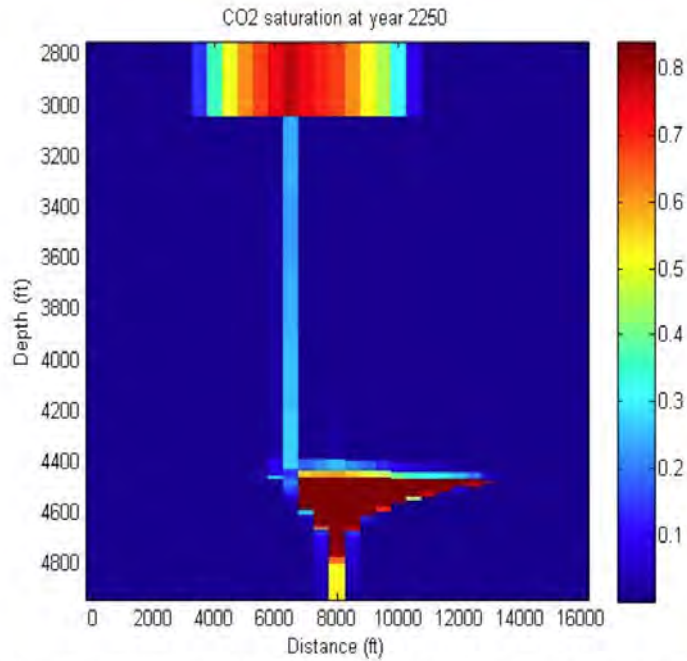


Figure 8: Cross section view of CO₂ saturation at the year 2250, notice the leaking up to the surface

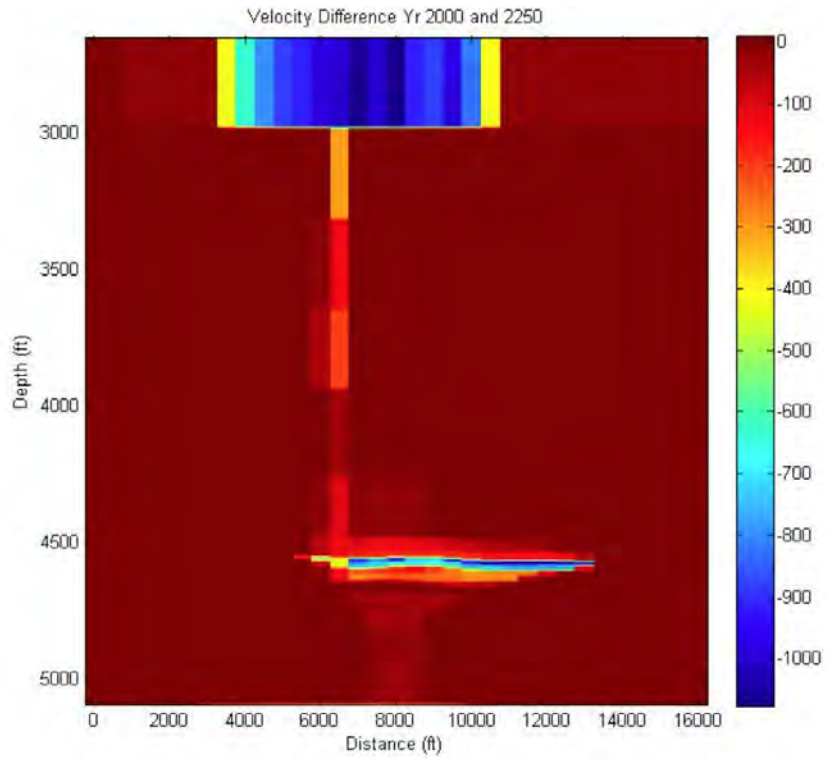
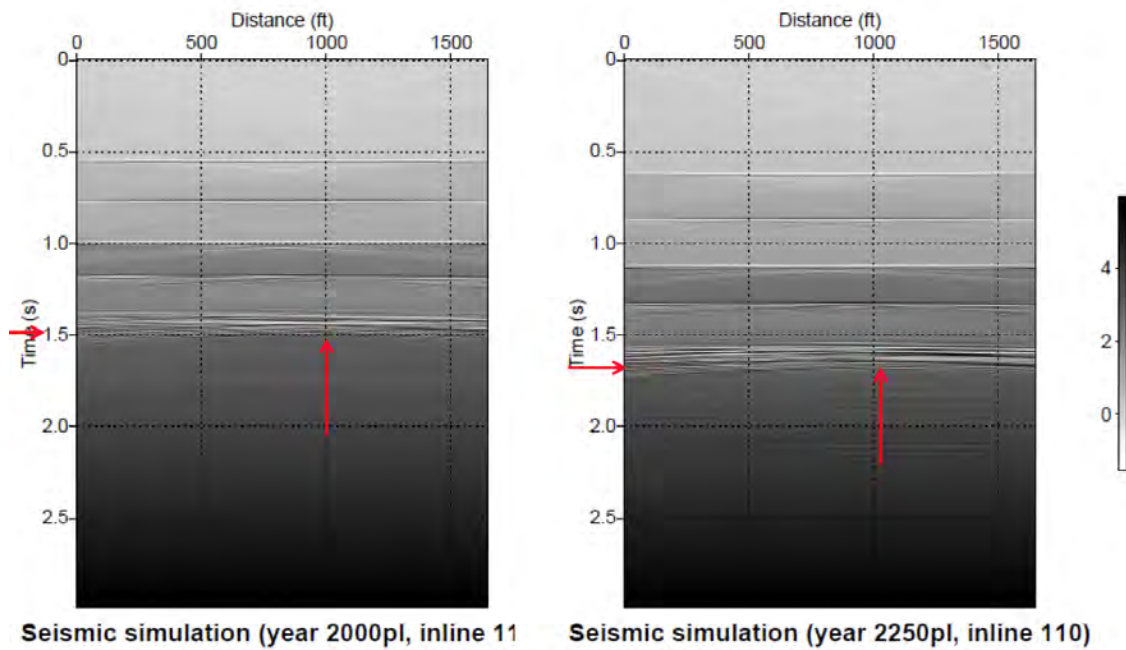


Figure 9 : Velocity difference due to CO₂ injection for year 2000' and 2250'



Seismic simulation (year 2000pl, inline 11) Seismic simulation (year 2250pl, inline 110)

Figure 10 : Difference of time shift and amplitude change on seismic due to CO₂ injection for year 2000' and 2250'

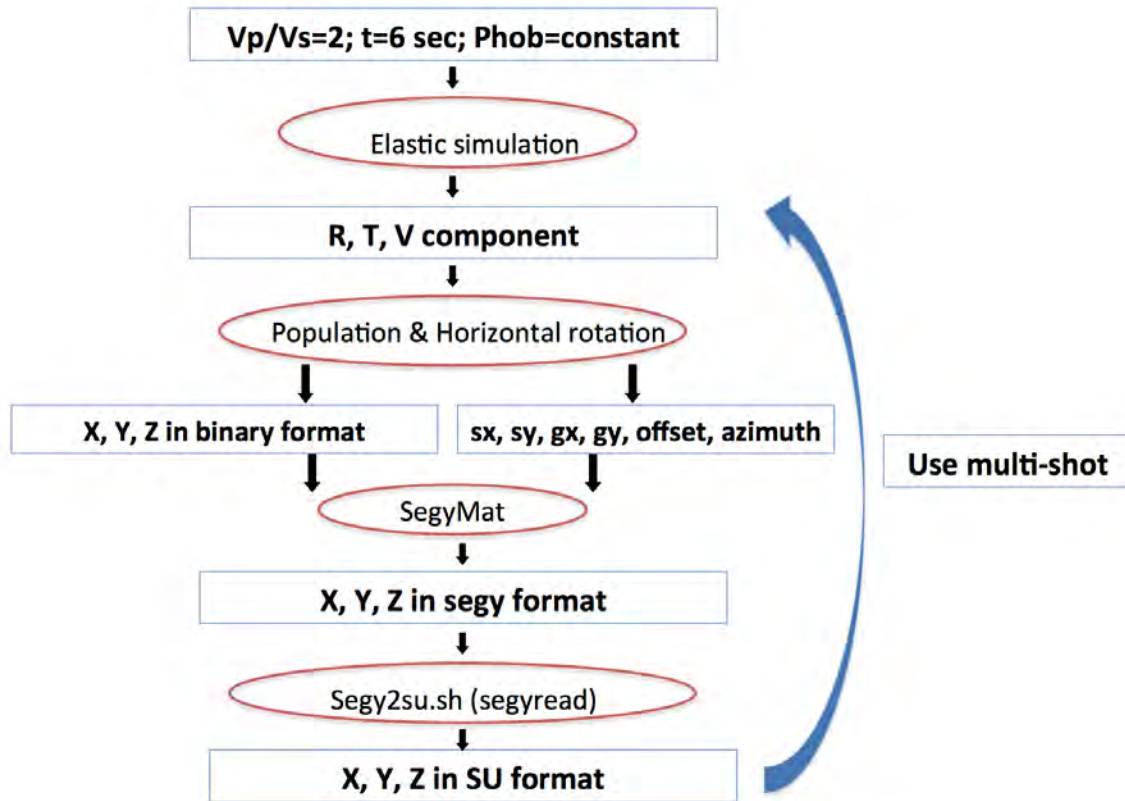


Figure 11. Flow chart

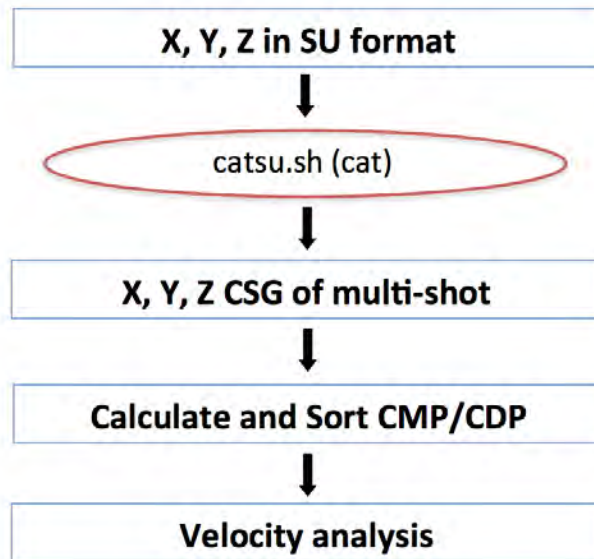


Figure 12. Continued flow chart

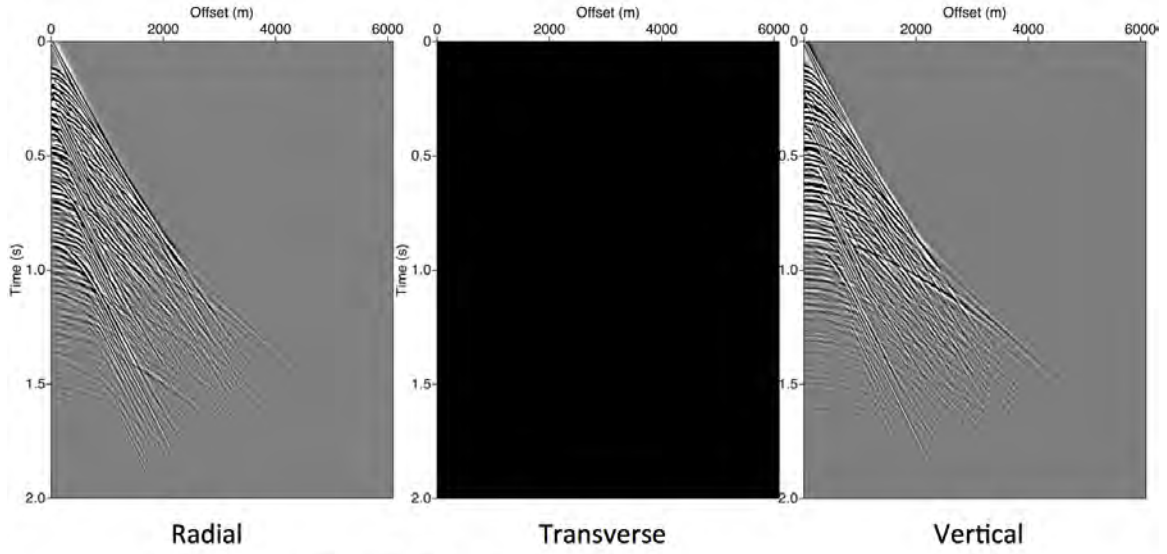


Figure 13. Radial, Transverse, Vertical component

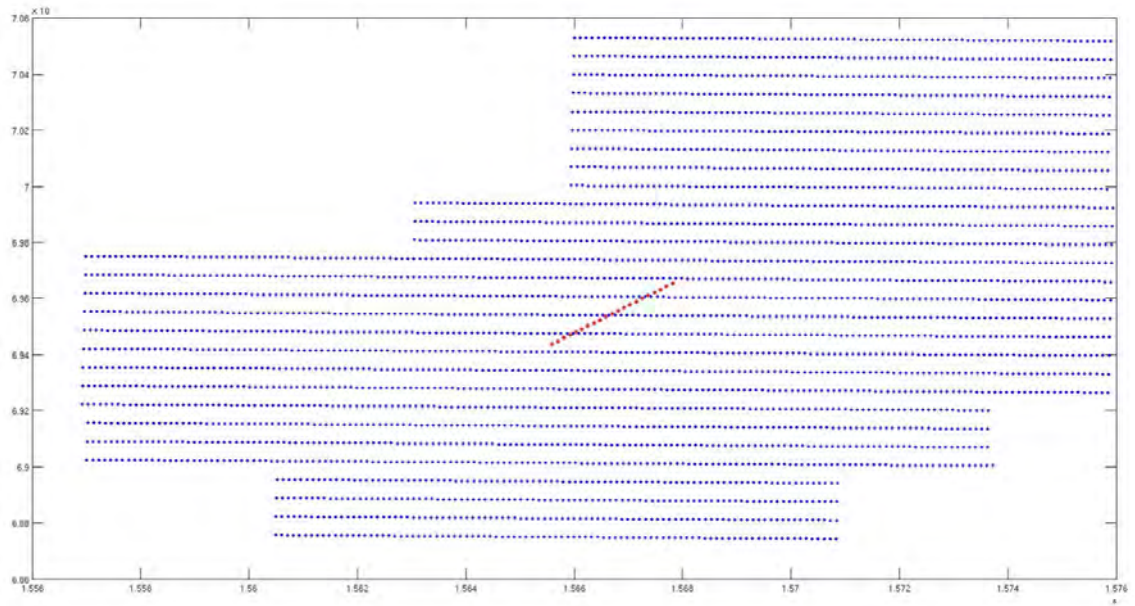


Figure 14. Geometry of receiver (blue dot) distribution and 21 simulated shots (red dot)

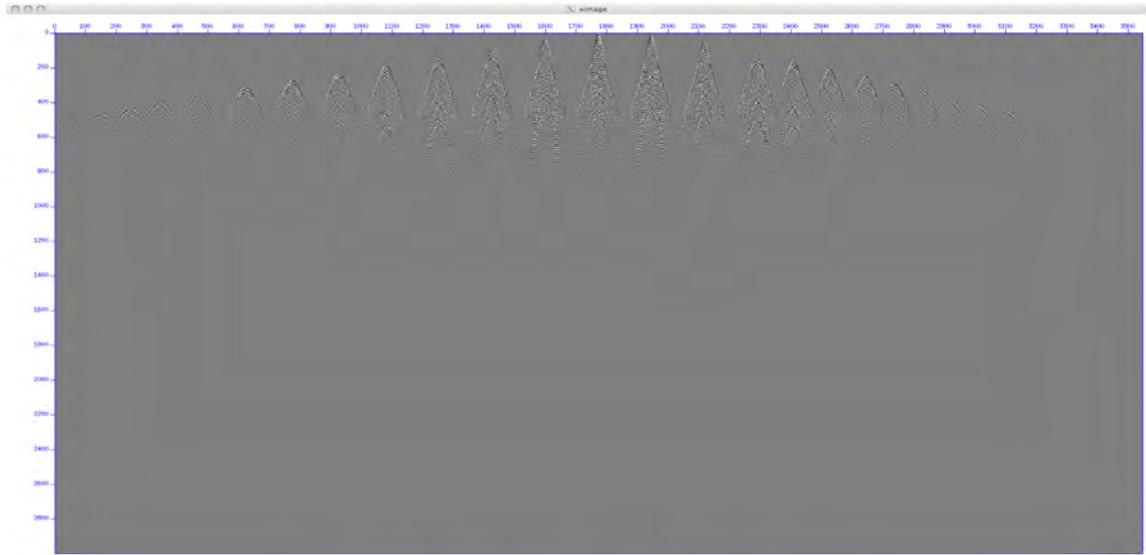


Figure 15a. X component of one shot (28 receiver lines)



Figure 15b. Y component of one same shot (28 receiver lines)

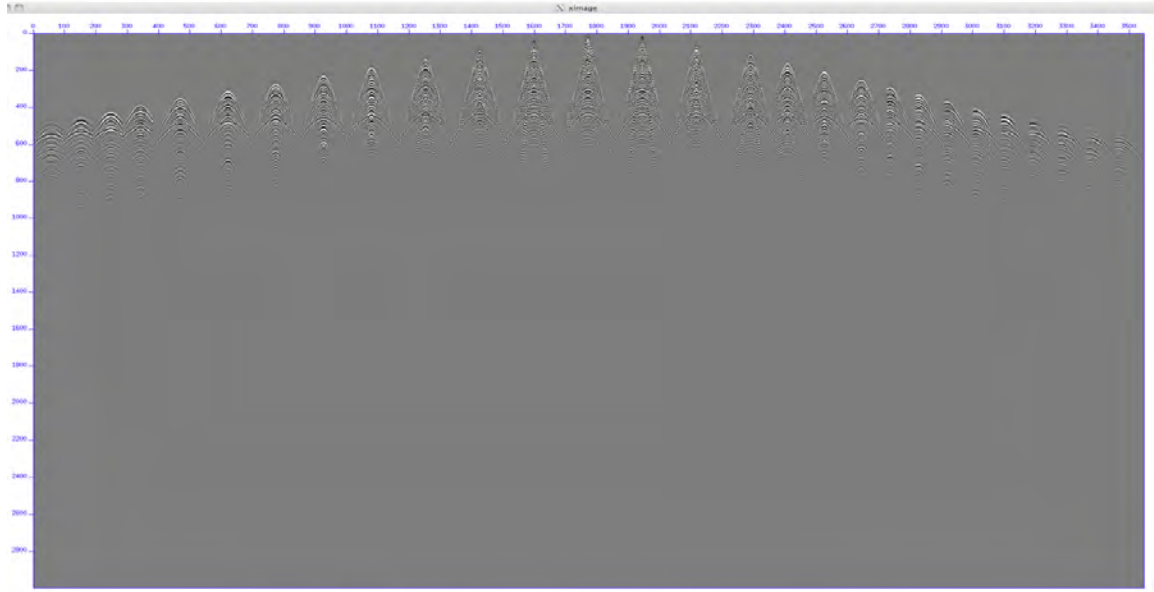


Figure 15c. Z component of same shot (28 receiver lines).

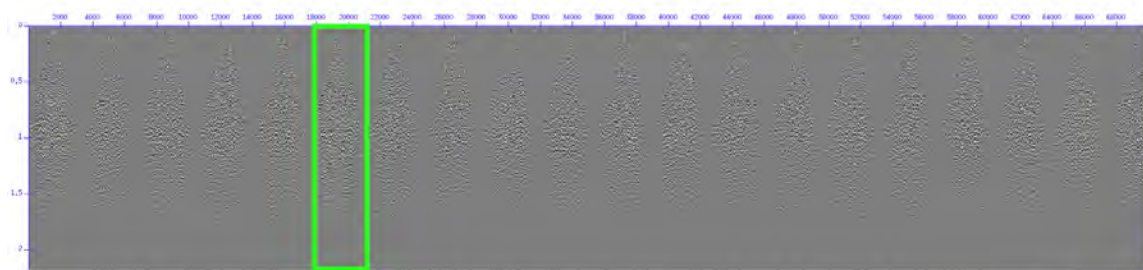


Figure 16. Concatenated X component of 21 shots. One unit in green box is for one shot, and there is 28 receiver lines in each shot.

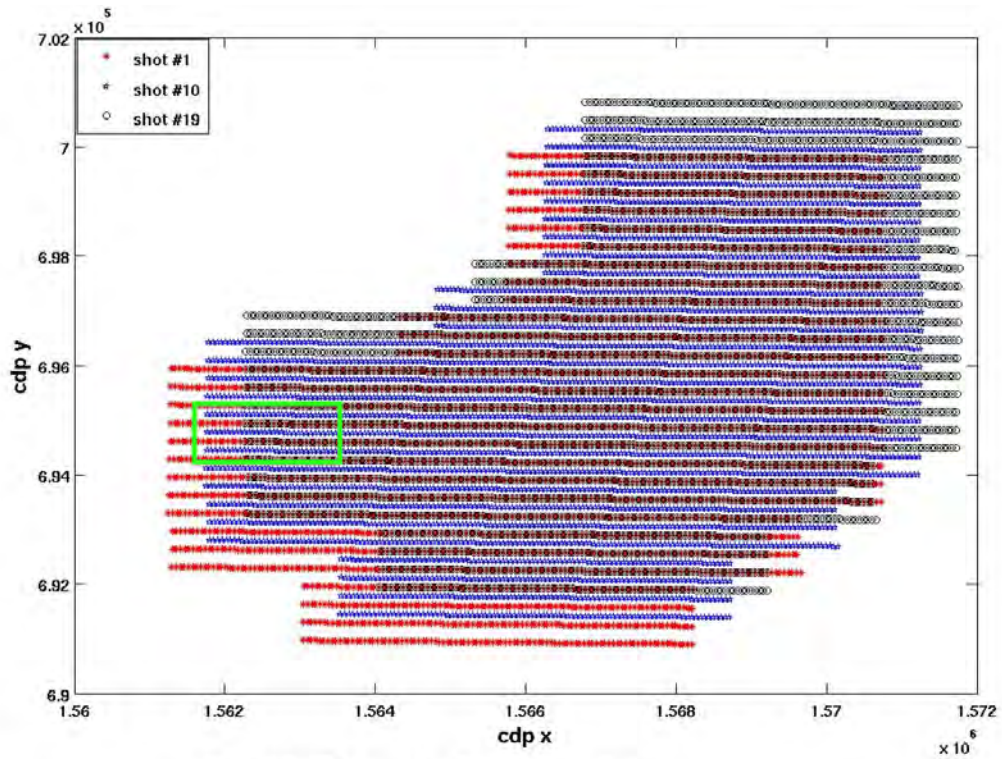


Figure 17. CDP geometry of 3 shots in one figure

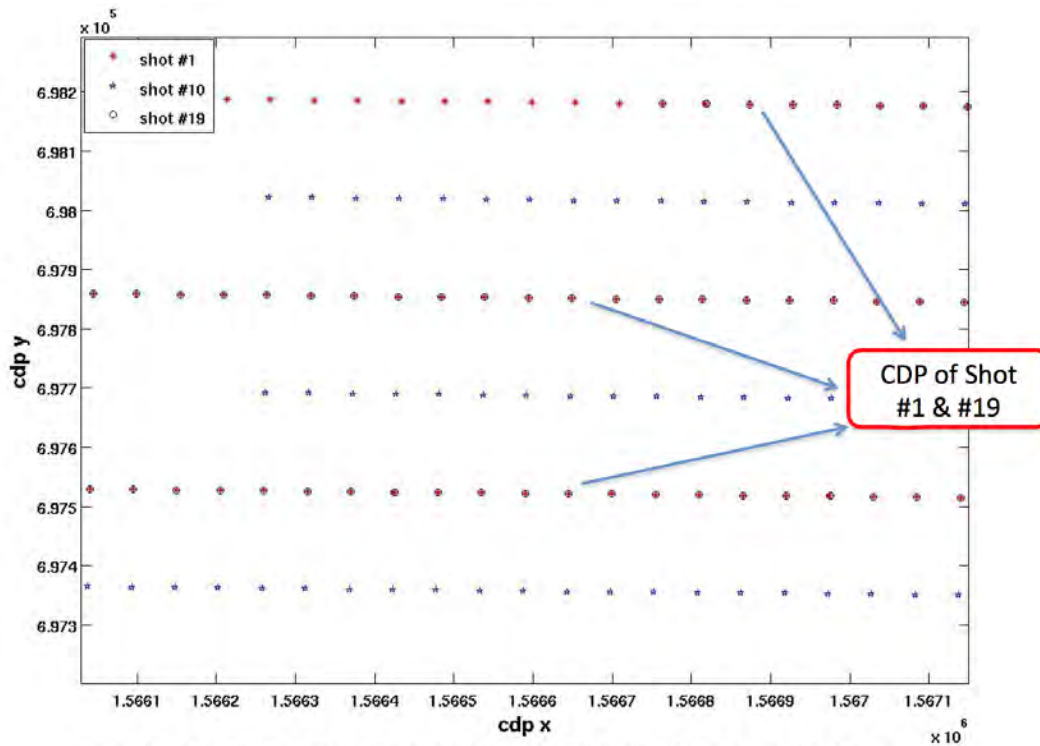


Figure 18. Zoom-in view of the green box in figure 7. CDP point of shot #1 and #19 fold up.

```

trace_number : 0 pick_time(s) : 0.007000
trace_number : 1 pick_time(s) : 0.006000
trace_number : 2 pick_time(s) : 0.007000
trace_number : 3 pick_time(s) : 0.007000
trace_number : 4 pick_time(s) : 0.007000
trace_number : 5 pick_time(s) : 0.007000
trace_number : 6 pick_time(s) : 0.007000
trace_number : 7 pick_time(s) : 0.006000
trace_number : 8 pick_time(s) : 0.006000
trace_number : 9 pick_time(s) : 0.006000
trace_number : 10 pick_time(s) : 0.007000
trace_number : 11 pick_time(s) : 0.006000
trace_number : 12 pick_time(s) : 0.007000
trace_number : 13 pick_time(s) : 0.007000
trace_number : 14 pick_time(s) : 0.007000
trace_number : 15 pick_time(s) : 0.007000
trace_number : 16 pick_time(s) : 0.007000
trace_number : 17 pick_time(s) : 0.007000
trace_number : 18 pick_time(s) : 0.006000
trace_number : 19 pick_time(s) : 0.007000
mean first pick time(s) : 0.006700
val : 0.000004
standard deviation for first pick time(s) : 0.000470

```

Direct Contact in AGL
(3-C transducer 1mhz)

Figure 19: SU result for direct contact in AGL with 1mhz 3-C transducer

```

trace_number : 0 pick_time(s) : 0.163000
trace_number : 1 pick_time(s) : 0.166000
trace_number : 2 pick_time(s) : 0.165000
trace_number : 3 pick_time(s) : 0.166000
trace_number : 4 pick_time(s) : 0.166000
trace_number : 5 pick_time(s) : 0.166000
trace_number : 6 pick_time(s) : 0.166000
trace_number : 7 pick_time(s) : 0.165000
trace_number : 8 pick_time(s) : 0.166000
trace_number : 9 pick_time(s) : 0.166000
trace_number : 10 pick_time(s) : 0.166000
trace_number : 11 pick_time(s) : 0.166000
trace_number : 12 pick_time(s) : 0.166000
trace_number : 13 pick_time(s) : 0.166000
trace_number : 14 pick_time(s) : 0.166000
trace_number : 15 pick_time(s) : 0.165000
trace_number : 16 pick_time(s) : 0.166000
trace_number : 17 pick_time(s) : 0.166000
trace_number : 18 pick_time(s) : 0.166000
trace_number : 19 pick_time(s) : 0.166000
mean first pick time(s) : 0.165700
val : 0.000010
standard deviation for first pick time(s) : 0.000733

```

KONG first break time in AGL
(3-C transducer 1mhz P)

Figure 20: SU result for 'KONG' sample in AGL with 1mhz 3-C transducer

```

trace number : 24
trace_number : 0 pick_time(s) : 0.126000
trace_number : 1 pick_time(s) : 0.127000
trace_number : 2 pick_time(s) : 0.127000
trace_number : 3 pick_time(s) : 0.127000
trace_number : 4 pick_time(s) : 0.127000
trace_number : 5 pick_time(s) : 0.127000
trace_number : 6 pick_time(s) : 0.127000
trace_number : 7 pick_time(s) : 0.127000
trace_number : 8 pick_time(s) : 0.127000
trace_number : 9 pick_time(s) : 0.127000
trace_number : 10 pick_time(s) : 0.127000
trace_number : 11 pick_time(s) : 0.127000
trace_number : 12 pick_time(s) : 0.127000
trace_number : 13 pick_time(s) : 0.127000
trace_number : 14 pick_time(s) : 0.127000
trace_number : 15 pick_time(s) : 0.127000
trace_number : 16 pick_time(s) : 0.127000 RPL Sample first break time
trace_number : 17 pick_time(s) : 0.127000 in AGL
trace_number : 18 pick_time(s) : 0.127000 (3-C transducer 1 mhz P)
trace_number : 19 pick_time(s) : 0.127000
trace_number : 20 pick_time(s) : 0.127000
trace_number : 21 pick_time(s) : 0.127000
trace_number : 22 pick_time(s) : 0.126000
trace_number : 23 pick_time(s) : 0.127000
mean first pick time(s) : 0.126917
val : 0.000002
standard deviation for first pick time(s) : 0.000282

```

Figure 21: SU result for RPL Sample in AGL with 1mhz 3-C transducer

DELINEATION OF SUBTLE GEOLOGIC FEATURES BY MULTI-ATTRIBUTE
SEISMIC ANALYSIS IN DICKMAN FIELD, KANSAS, A POTENTIAL SITE FOR
CO2 SEQUESTRATION

Presented to
The Faculty of the Department of Earth and Atmospheric Sciences
University of Houston

In Partial Fulfillment
Of the Requirements for the Degree
Masters of Science
Geophysics

By
Heather King
December, 2011

Introduction

CO₂ sequestration could significantly reduce the amount of CO₂ in the atmosphere. Sequestration is the process of injecting CO₂ into a storage location. In order for sequestration to make a substantial difference in the amount of CO₂ in the atmosphere, a site must be able to successfully store and trap CO₂ for thousands of years. There are several potential storage locations including terrestrial, ocean, and geologic sites as shown in Figure 1 (Hilterman and Bjorklund, 2007). Geologic sequestration sites include unminable coal beds, saline formations, and depleted oil and gas reservoirs. Saline formations and depleted petroleum reservoirs make good sites for possible CO₂ sequestration because of their inherent seal integrity.

The Reservoir Quantification Laboratory (RQL) is currently in the late stages of a study assessing four geological reservoirs for potential CO₂ sequestration (Hilterman and Bjorklund, 2007). They are located in Wyoming, Kansas, Ohio, and Illinois (Figure 2). The aim of this study is to simulate CO₂ injection by creating very accurate and detailed reservoir models with the use of well log data, production data, and seismic data. My study concentrates on the Kansas site which is the Dickman Field in Ness County.

The Dickman Field reservoir of interest is part of the Lower Paleozoic Ozark Plateau aquifer system which extends into nine states and is composed of fresh water and saline portions (Figure 3) (Nissen et al. 2004). The saline portion is known as the Western Interior Plains aquifer system and extends throughout the state of Kansas. The Western Interior Plains system is made of a Mississippian-aged carbonate formation that has been modified by karst processes and is known to be highly fractured. The formation is unconformably overlain by shale of Pennsylvanian age and was created from channels,

which deposited channel sands that are part of the aquifer (Figure 4). This interval of carbonates and sandstones is associated with oil and gas throughout Kansas.

The Dickman Field reservoir is a good candidate for study because of its proven seal integrity and potential storage capacity, which has been predicted to be near 1MtCo₂. It is representative of many reservoirs throughout the mid-continent and its small size allows for a comprehensive and complete study. In order to better understand the processes and factors dictating reservoir characteristics, more detailed geologic models and further attribute analysis needed to be completed. The seal of a reservoir is key in its potential to store fluids. Detailed and accurate depth maps and an extensive study of the currently available attributes can give a lot of insight into the nature of this reservoir's seal.

Many of the subtle geological features present in the Mississippian formation have been delineated through seismic amplitude and attribute data. The hypothesis of this thesis is that detailed and accurate maps and an extensive study of the currently available attributes can determine if these features are also present in the seal, which is proposed to be within the Marmaton group. The Fort Scott Limestone which is about 150 ft. above the Mississippian is a formation top that was consistently identified in many of the well logs and was chosen to represent the seal of the reservoir. Determining if these features persist into the seal and how they may currently affect the seal is important in understanding how these features could affect flow within and out of the reservoir, locations for drill sites, as well as potential hazards. Background information, typical interpretation with seismic amplitude and well data, and interpretation of the available

attributes is presented below with an emphasis on the seal of the reservoir, the Fort Scott Limestone.

Geology

Lithology

The Marmaton Group, which is stratigraphically directly above the Cherokee Group, has been described based on outcrop descriptions from a large belt (10 to 25 miles in width) of outcrops along the Kansas-Missouri boundary as shown in Figure 5(Moore, 1949). The Fort Scott Limestone is the lowest formation in the Marmaton Group. It extends throughout Kansas, Oklahoma, Missouri, Iowa, and Nebraska in the subsurface and in outcrop and classification varies from state to state based on stratigraphic differences and historical nomenclature. For this discussion, the formation definitions and descriptions outlined in Moore(1949), which are generally accepted throughout Kansas, and have been adapted by Zeller(1968), and Merriam(1963), will be followed. Moore(1949) defines the Fort Scott Limestone formation to be composed of 2 limestone members separated by a shale with the total formation thickness ranging from 13-145 feet with an average of about 30 feet throughout Kansas(Merriam,1963).

The upper member is the Higginsville Limestone which is light to dark gray with a medium-grained crystalline texture and a brecciated appearance. Irregular wavy beds and stems of fusulines and large crinoids are found throughout the member and the upper portion is mostly made up of a coral called Chaetetes.

The middle member is the Little Osage Shale which is a grey to black fissile shale with an interbedded layer of coal in the lower section and a very thin limestone in the

middle. Both are less than 1 foot in thickness in Kansas. Fossils are scarce throughout the member.

The lower member is more variable depending on location, but can generally be described by an upper portion that is light gray with a coarse crystalline texture and irregular bedding and a lower part that is tan, brownish, or dark gray fossiliferous limestone with thicker, more regular bedding than the upper portion and is commonly found to have conchoidal fracture. The upper portion contains Chaetets and fusulines while mollusks are common in the lower portion.

Depositional Environment

The Marmaton Group, as well as the Cherokee Group stratigraphically above it, are dominantly composed of stratigraphic sequences of marine and nonmarine deposits indicative of numerous advances and retreats of a shallow sea. Throughout both groups, the sequences approximately follow the following order, taken directly from

Merriam(1963)

“(1) nonmarine sandstone, commonly uneven at the base, occupying channels cut in subjacent rocks, (2) sandy, silty, and clayey shale, unfossiliferous or containing land plant remains, (3) underclay, (4) coal, (5) black platy shale containing conodonts, and commonly bearing small spheroidal phosphatic concretions, (6) gray to brownish clayey or calcareous shale, or limestone containing a varied assemblage of marine invertebrates.”

While sequences often lack certain lithologies from the above description, the order of appearances is generally followed throughout the Marmaton group and Cherokee group, indicating consistent depositional cycles throughout both groups.

The fossiliferous limestone portions of the Fort Scott Limestone are indicative of the latest stage of an advance of a shallow sea and the intervening shale portion would indicate slight retreats of the sea before further advancement allowing deposition of the overlying upper unit of the Fort Scott.

Directly below the Fort Scott Limestone is a black shale which marks the uppermost part of the Cherokee Group. Other formations of the Marmaton Group extend above the Fort Scott Limestone and follow the same cyclic layering of nonmarine and marine sedimentation.

Tectonic History

Directly below the Fort Scott Limestone is a black shale which marks the uppermost part of the Cherokee Group. Other formations of the Marmaton Group extend above the Fort Scott Limestone and

The tectonic history of Kansas is relatively simple because Kansas is located on a platformlike extension of a large, stable craton(Merriam, 1963). A thin layer of sedimentary rock covers the basement complex which has had a limited amount of structural deformation and consists of thin units that lay nearly parallel and horizontal.

The Dickman Field is located on the Southwest flank of the Central Kansas Uplift(CKU) as shown in figure 6(Gerhard, 2004). The CKU is a region of uplift that trends northwest and is most likely associated with the plate convergence along the Ouachita Mountains orogenic belt in Arkansas when North America collided with

Gondwanaland from the Southeast. This deformation occurred from the late Mississippian to early Pennsylvanian and is considered the latest major structure deformation to affect the region (Merriam, 1963). Faults and fractures interpreted from oil drilling, drainage patterns, and smaller scale surface structures indicate the presence of NW- and NE-oriented faulting and fracturing in the study area.

Interpretations

Dickman 3D Seismic Attributes Generation

19 attributes have been generated by Geokinetics from the full offset Dickman 3D seismic dataset. Parameters for attribute generation were determined based on acquisition and processing parameters, physical properties of the target area, and resolution limits of the data. Variable parameters, those based on physical properties and resolution limits of the data, were chosen based on test images of curvature. All others were invariable because they were set by acquisition and processing parameters. Table HK.1 lists the parameters used for attribute generation and for all available data sets acquired thus far.

Seismic attribute analysis has been used to link geologic features, such as faults, fractures as well as to determine hydrocarbon deposition, generation, migration, entrapment, etc. Seismic amplitude extraction of dip azimuth and magnitude can directly provide a quantitative measure of the structural characteristics. Coherence, curvature and ant tracking volumes can detect the small scale and subtle change in seismic reflections

that are below seismic amplitude resolution. The following gives a list of attributes that have been used for the Dickman field.

The following attribute sections will be accompanied by attribute maps for the Mississippian and Fort Scott Horizon. Each map contains interpretations in green, which were made by evaluating all of the attributes together.

Amplitude

Seismic amplitudes can be calculated in different ways, such as maximum peak and minimum trough, average, RMS(root mean square),etc. They are extracted from a user-defined time window generally on a picked time horizon. An amplitude anomaly can be a direct indicator of hydrocarbons. It's very sensitive to the seismic reflections due to impedance contrast of the adjacent sedimentary layers.

Figure 7 shows amplitude maps for the Mississippian and Fort Scott horizons. Within the Mississippian, some lineations are visible as well as a channel running through the dataset. However, since amplitude is sensitive to many variables and has limited resolution, many features that show up in other attributes are not visible in the amplitude map. The channel interpretations correlate well with the edges of high amplitude packages and a fault in the north correlates well with a low amplitude lineation.

The Fort Scott horizon also shows the north fault as well as a possible extension of the fault in the east, a few other lineations as well as a small dark package that may correlate to channel in the Mississippian horizon.

Time Gradients

Time gradient attributes are straight forward calculations based on an amplitude data set. The gradient is simply the change in time over a certain distance of a reflection. These calculations are done by fitting a plane through a reflection and calculating the dip and azimuth of the plane from the point of interest. This is illustrated in Figure 9. The dip refers to the magnitude and the azimuth refers to the direction. The gradient can be calculated in many different directions including along the inline direction, crossline direction, and the direction of maximum dip or magnitude (Rijks and Jauffred, 1991).

These attributes are viewed better on horizons than on time slices. They give insight to the geometry of a surface, and can help delineate any features that have changed the shape of the formation interfaces represented by the reflections. The following datasets have been calculated from the Dickman 3D amplitude dataset by Geokenetics: dip in the crossline direction (crossline dip), magnitude in the crossline direction (crossline gradient), dip in the inline direction (inline dip), gradient in the inline direction (inline gradient), direction of maximum dip (dip azimuth), magnitude of maximum dip (dip magnitude), direction of maximum gradient (grad azimuth), and magnitude of maximum gradient (grad magnitude).

A dip map measures magnitude of local dip (ms/m or ms/ft), e.g. the inclination of a horizon. Dip azimuth measures angle in degrees from local reference directions and dip magnitude (the magnitude of maximum dip). Rijks and Jaufred (1991) showed that horizon-based dip magnitude and dip-azimuth are useful in delineating subtle faults whose displacements measure only a fraction of a seismic wavelet. They can help to

determine fault locations, subtle trace to trace vertical shift, minor faults or flexures, stratigraphic features such as channels, small-scale reservoir disturbance, etc.

A gradient magnitude operator detects the amplitude edges at which pixels change their gray-level suddenly. For an image volume $f(\mathbf{x})$, the magnitude of the gradient vector is:

$$|\nabla f| = \sqrt{\left(\frac{\partial f}{\partial x}\right)^2 + \left(\frac{\partial f}{\partial y}\right)^2 + \left(\frac{\partial f}{\partial z}\right)^2} \quad (1)$$

assuming a local maximum at an amplitude edge. The amplitude along the enhanced discontinuity surface varies irregularly depending on the amplitude contrast of the adjacent sedimentary layers. This can be used to detect amplitude change due to fault or fractures.

Figure 10 shows the dip azimuth map for the horizons. Areas of similar azimuth direction show up in the same color. This map is difficult to interpret on it's own but is easier in conjunction with the magnitude map which is shown in Figure 11.

On the Mississippian maps, when the dip magnitude changes within the channel, the dip azimuth also changes slightly. The edges of the channel do not correlate with highest dip or a certain dip direction, rather, it correlates in areas where the dip changes from a high dip to a low dip. The northern fault falls in a break between large areas of constant dip. To the northwest of the fault, the dip is consistently around 50 degrees with high magnitude and to the southeast, the dip is consistently around -50 degrees and of much lower magnitude. The Fort Scott horizon maps show similar characteristics for the fault. No other features appear to have significance in these maps.

Figures 11 and 12 show similar maps, however now they show the azimuth and magnitude of the gradient. These maps are even more difficult to interpret as the maximum gradient is dependent on both magnitude and direction. However, these maps show similar behavior for the fault. The channel appears to have varying azimuths on the channel depending on location on the channel and the gradient tends to be highest along the edges.

Coherence

The use of coherence on 3D seismic data was developed in the early 1990's by Bahorich and Farmer for quantifying waveform similarity between neighboring traces (Chopra and Marfurt, 2005). This was done by computing a localized, normalized cross-correlation of adjacent traces. For example, if a set of seismic traces are cut by a fault, the undisturbed traces on either side of the fault have very high continuity, while the trace(s) affected by the fault will produce a low correlation coefficient at that point (Bahorich and Farmer, 1995). This would lead to a discontinuity in the coherence, producing a lineation of low coherence along the fault.

Another method to calculate coherency is semblance- or variance-based. Semblance is the energy ratio of the average of the traces along a specific dip to the trace.. Variance is simply 1 minus the semblance. Figure 16 diagrammatically shows how this is done. Figure 16(a) shows the original traces within a specific window and dip, 16(b) shows the average of these traces, and 16(c) shows how the traces are all replaced with a scaled version of the average that best fits the original trace (Chopra and Marfurt, 2007). The semblance is the ratio of figure 16(c) to figure 16(a). Similar to

crosscorrelation-based coherency, where there are low similarities between a trace and the average trace, a high discontinuity will be produced (Chopra and Marfurt, 2007).

This attribute will delineate geological features, such as faults, channels, fractures, and other stratigraphic boundaries by highlighting subtle differences between neighboring traces. In traditional 3D interpretation, such features can become difficult to view at certain alignments relative to bedding and viewing orientation. Since coherence will suppress laterally coherent features such as bedding, these features will be exemplified regardless of their orientations. Bahorich and Farmer demonstrated that while some of these features can appear more in focus in attributes such as dip and azimuth, coherence tends to give a more accurate portrayal, being independent of how well a horizon has been interpreted.

The coherent energy gradient can also be effective in delineating lateral changes in rock thickness, which are expressed in seismic data as changes in thin bed tuning (Marfurt, 2004).

Figure 15 shows maps showing total energy, which are equivalent to figure 16(c). This map shows average energy over a window of 10 ms. Different lithologies, thicknesses, reservoir characteristics etc will produce different levels of energy. The darker the color, the higher the energy. This map looks very similar to the amplitude map but with poorer resolution. Small features, such as the acquisition footprint in the amplitude map, is no longer resolvable. Figure 16 is analogous to the ratio of 14(c) to 14(a) which is the energy ratio or semblance. Areas where the magnitude of the average energy is greater than the original trace energy show up as light and dark extremes. This means that areas of discontinuity or low magnitude energy ratio show up in greys. So,

features that correlate with discontinuities such as channel edges, faults and fractures lie in changes from light to dark. The fault can be seen in both horizons as a light lineation and the channel package is highly differentiable in the Mississippian horizon.

Curvature

Curvature is defined as the deviation of a surface from a straight line. In other words, it is the rate of change of direction of a curve at a certain point, which is the second derivative of the curve. It can also be described as the inverse of the radius of a circle that fits the curve at that point, such that a straight line will produce zero curvature, a synform produces a negative curvature, and an antiform produces a positive curvature. This can be extended into 3 dimensions by using a surface instead of a line and an ellipsoid instead of a circle. Since the surface at a point can have different curvatures at different azimuths, an ellipsoid is used instead of a sphere (Roberts, 2001).

Figure 17 illustrates the naming conventions for the different possible curvatures for the 3-dimensional case (Roberts, 2001). The curvatures along the surface's dip and strike are known as the dip curvature and strike curvature. These curvatures will always be orthogonal to each other, as will the maximum and minimum curvatures. The maximum curvature is defined as the surface of an orthogonal plane that intersects the surface at the azimuth with the maximum curvature, or where a circle of the smallest radius would fit the curve. The minimum curvature is not necessarily the plane with the smallest curvature on the surface, it is simply the plane orthogonal to the maximum curvature. The maximum curvature can be calculated for both positive and negative curvatures, giving two independent volumes. A large number of combinations of these

curvatures can create varying curvatures, but this study focuses on maximum curvatures (Roberts, 2001).

Since curvature describes the shape of a reflection, it is essentially linked to the structure of the subsurface. Curvature should be able to illuminate any geological feature that dictates the shape of a reflection such as channels, faults, fractures, karst modifications, meteor craters, and volcanoes. These features could have affected the rocks when the interface represented by the reflection was at the surface of the earth or after burial.

Four curvature datasets have been created from the Dickman 3D amplitude dataset. These include maximum curvature, minimum curvature, most positive curvature and most negative curvature.

Figure 18 shows the positive curvature maps where high magnitudes of curvature are shown in black. Figure 19 shows the negative curvature maps where high magnitudes of curvature are shown in white. Interpreted features do not correlate with high magnitudes in either map, but instead seem to correlate with certain edges. Therefore, it is useful to look at curvatures together on one map. Figure 20 shows maps showing positive curvature in red, negative curvature in blue and energy ratio in grey scale. Now it is obvious that features correlate well between areas of high magnitude curvature. The green interpretations can now be more accurately placed showing where the fractures, faults, and channel features lie.

Conclusion

The Dickman Field is a good site to study in regards to its capacity to potentially store CO₂ because of its small size, availability of data, and the applicability to many midcontinent reservoirs. Data sets have been compiled and typical interpretation has been completed. Further analysis and interpretation of the seismic data has been conducted to delineate certain features within the seal of the reservoir.

The seismic attributes available in the Dickman Field data set have been used to more accurately interpret both the Mississippian and Fort Scott horizons. The Mississippian horizon contains a known channel as well as a fault and many fractures. The extent of faulting and fracturing in the seal of the reservoir, the Fort Scott horizon, was previously unknown. The interpretations shown above indicate that while there is some fracturing and faulting in the Fort Scott, it is not nearly as extensive as it is in the Mississippian. Further work including more data acquisition and processing and interpretation of other available attributes could lead to even further delineation of these features. Modeling that includes the interpreted features could lead to a better understanding of the significance of the features on the reservoir's ability to act as a CO₂ storage container and flow within the reservoir.

Figures

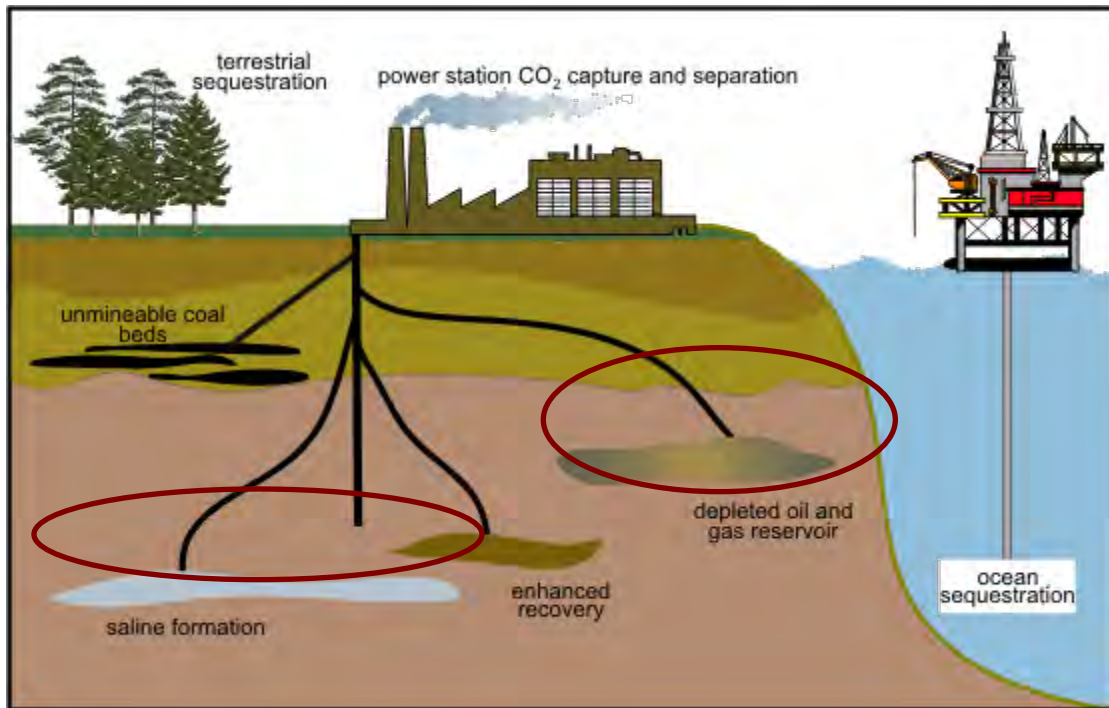


Figure 1: Diagram showing the possible types of CO₂ sequestration. Saline formation and depleted oil and gas reservoir are circled in red and are the focus of the RQL CO₂ sequestration study. Both types make good potential sites because of their known seal integrity. <http://www.eia.doe.gov/kids/classactivities/images/carbon%20sequestration.gif>

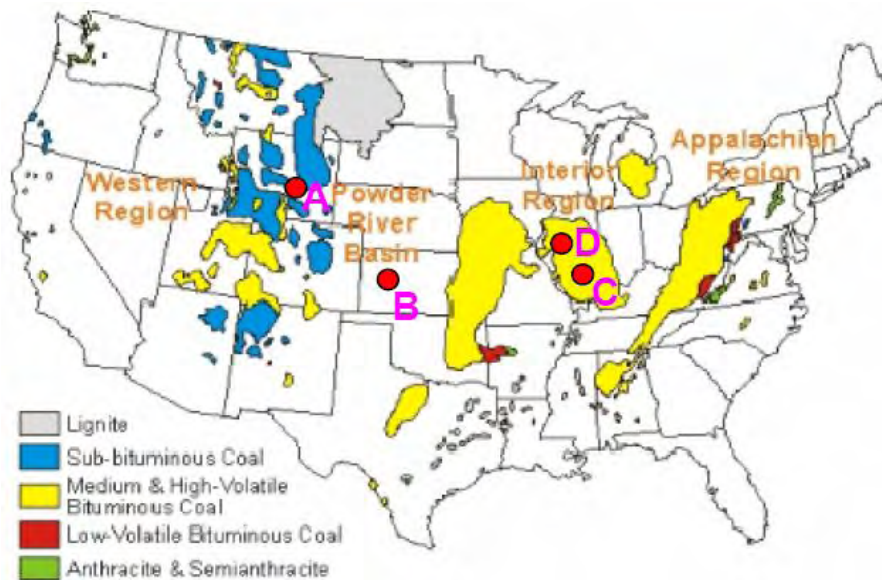
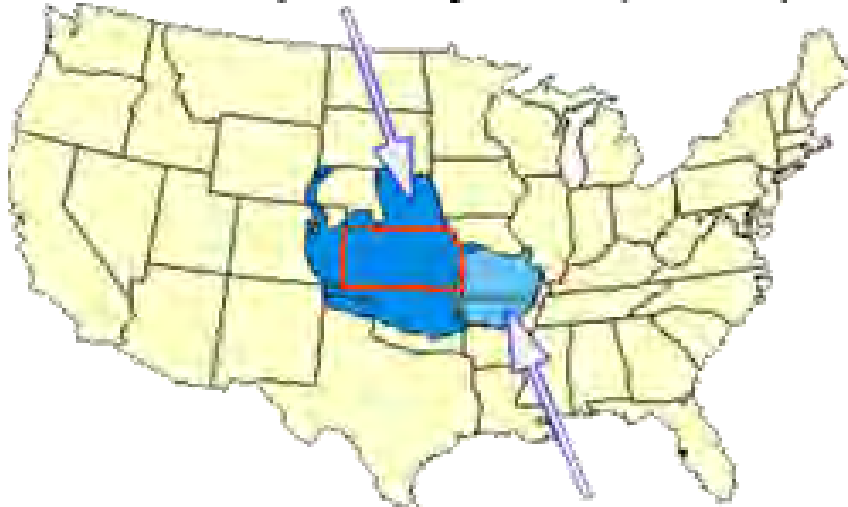


Figure 2: Map showing the RQL sites which are (A) Wyoming, (B) Kansas, (C) Ohio, and (D) Illinois (Hilterman and Bjorklund, 2007).

Western Interior Plains aquifer system (saline)



Ozark Plateaus aquifer system (freshwater)

Figure 3: Map showing the Lower Paleozoic Ozark Plateau aquifer system that extends into 8 states and has a saline portion called the Western Interior Plains aquifer system (Nissen, Marfurt, Carr, 2004).

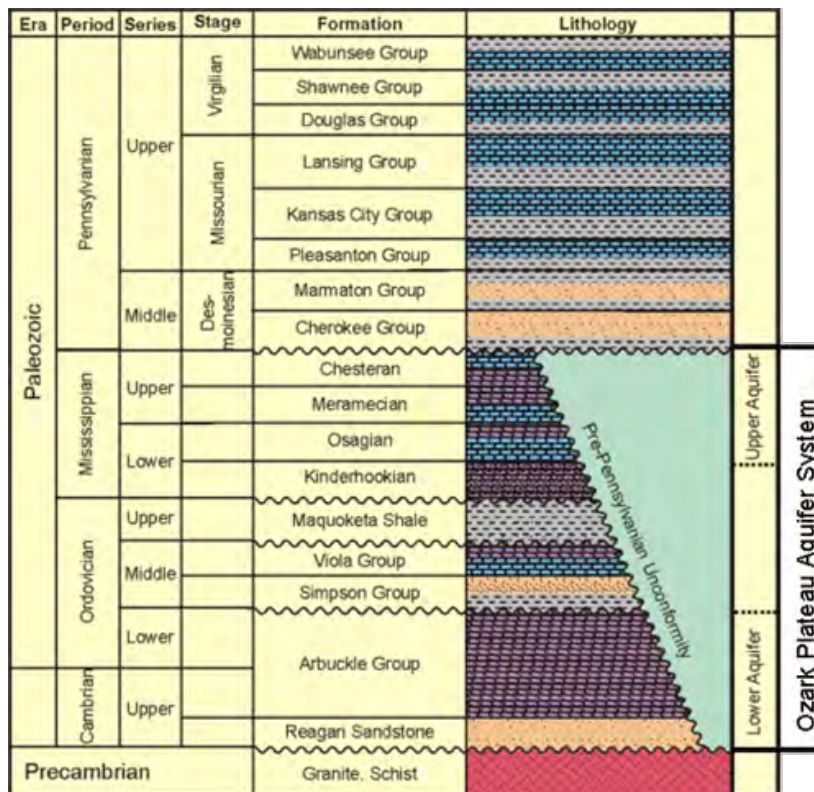


Figure 4: Stratigraphic section showing the Lower Paleozoic Ozark Plateau aquifer system which is made up of a Mississippian carbonate that is unconformably overlain by a Pennsylvanian shale (Nissen, Marfurt, Carr, 2004).

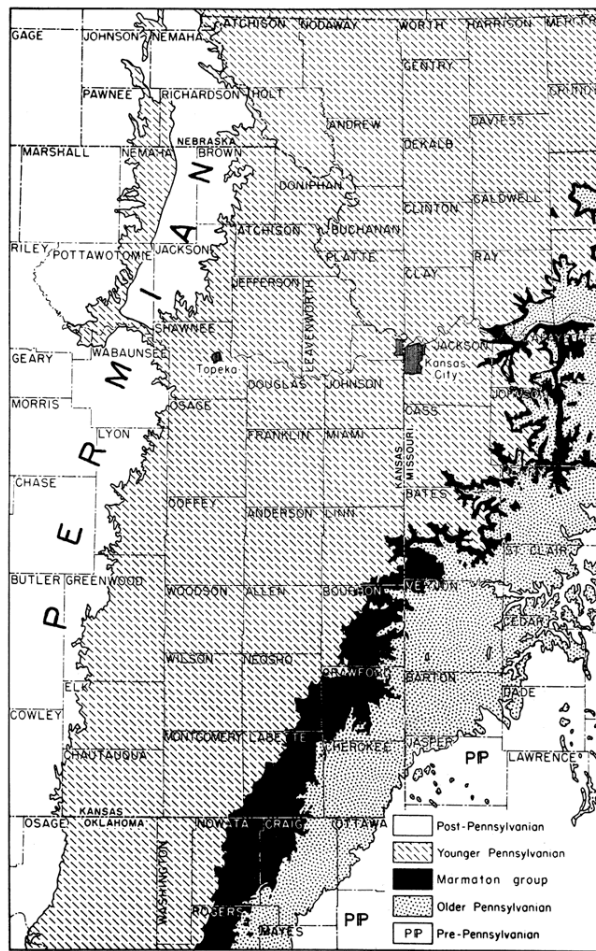


Figure 5: Distribution of Marmaton outcrops in Kansas and parts of adjoining states. The Marmaton group comprises the upper part of the Desmoinesian Series of Pennsylvanian rocks in the northern midcontinent region. (Moore, 1949)

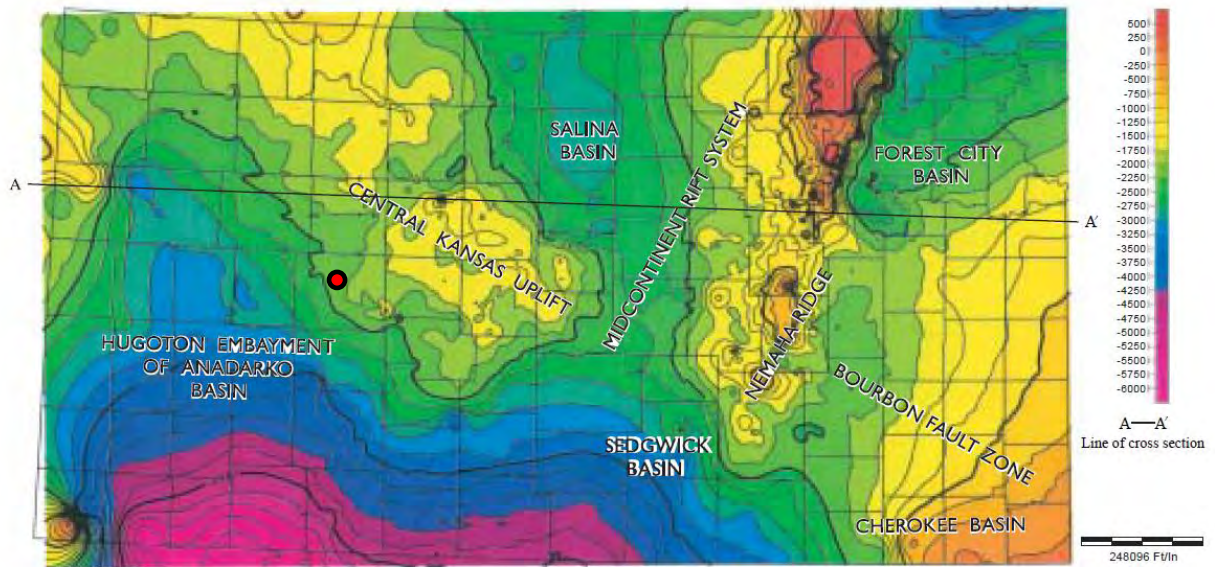


FIGURE 4. Map showing topographic (structural) relief on the present Precambrian/Phanerozoic surface. Major geologic structures of Kansas are labeled (T. Carr, personal communication, 2003). A-A' is line of section for fig. 5.

Figure 6: map showing topographic relief and the location of Dickman F field with respect

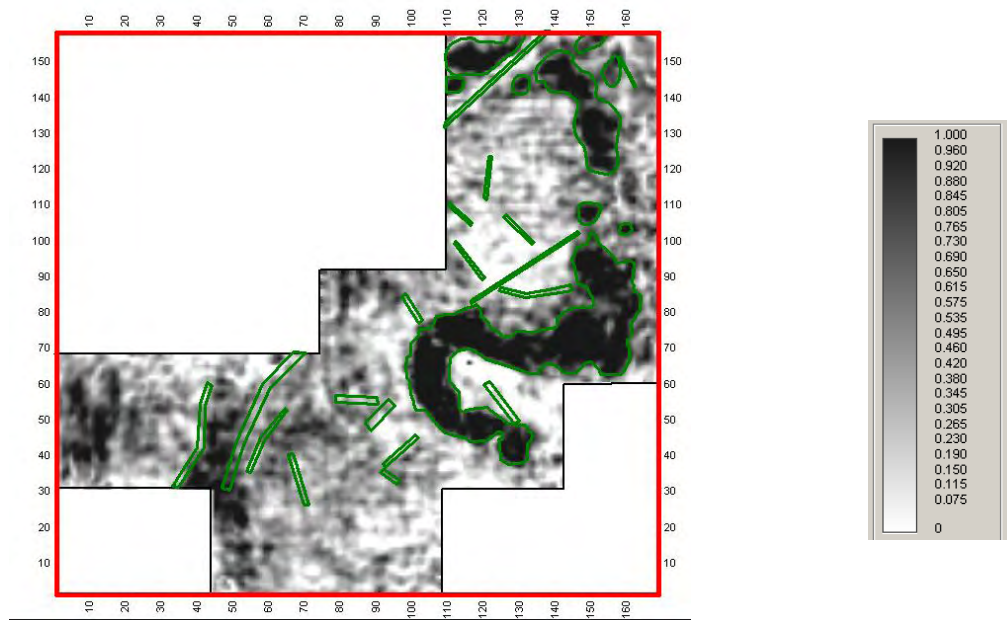


Figure 7: Seismic amplitude map extracted from the Mississippian horizon.

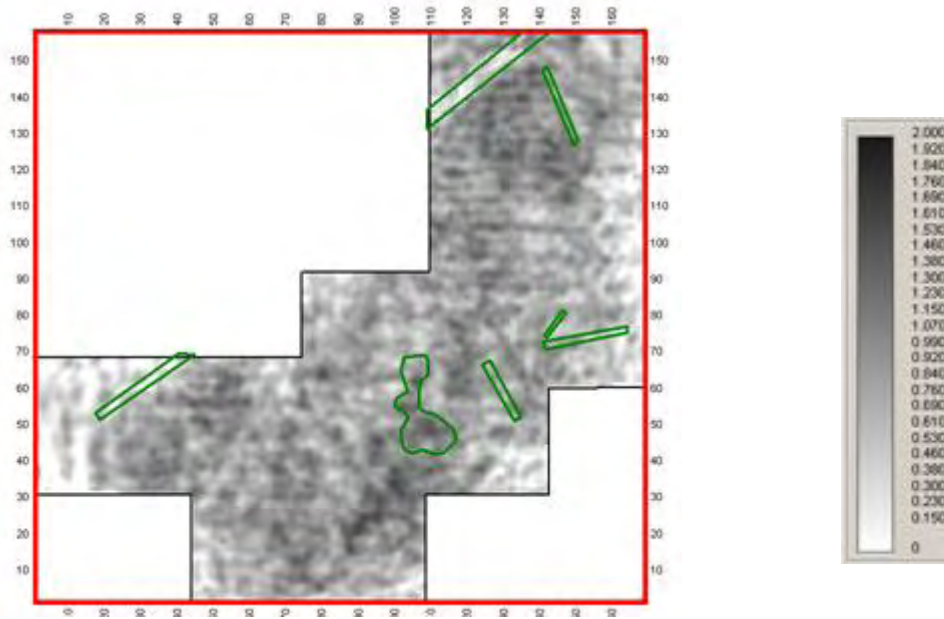


Figure 8: Seismic amplitude map extracted from the For Scott horizon.

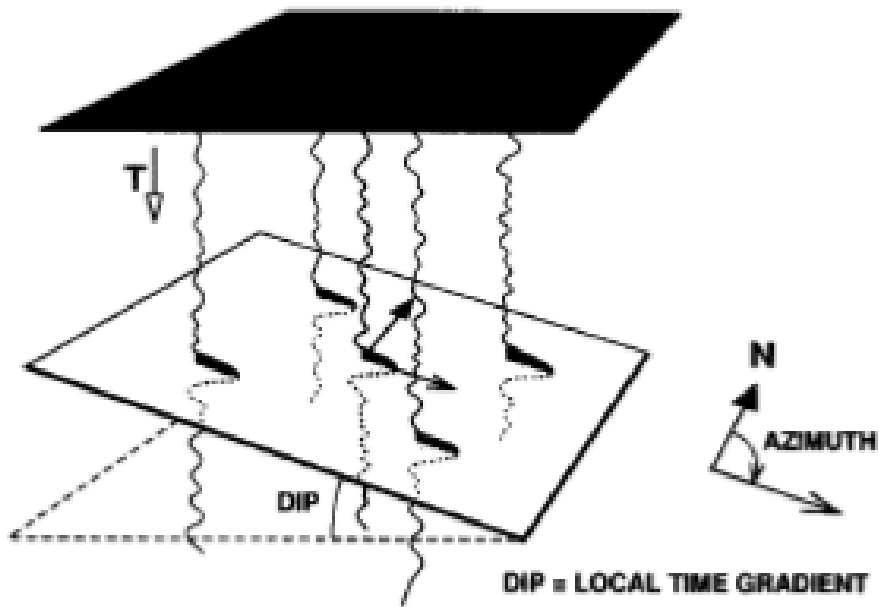


Figure 9: Diagram showing the principle of dip and azimuth calculation (Rijks and Jauffred, 1991).

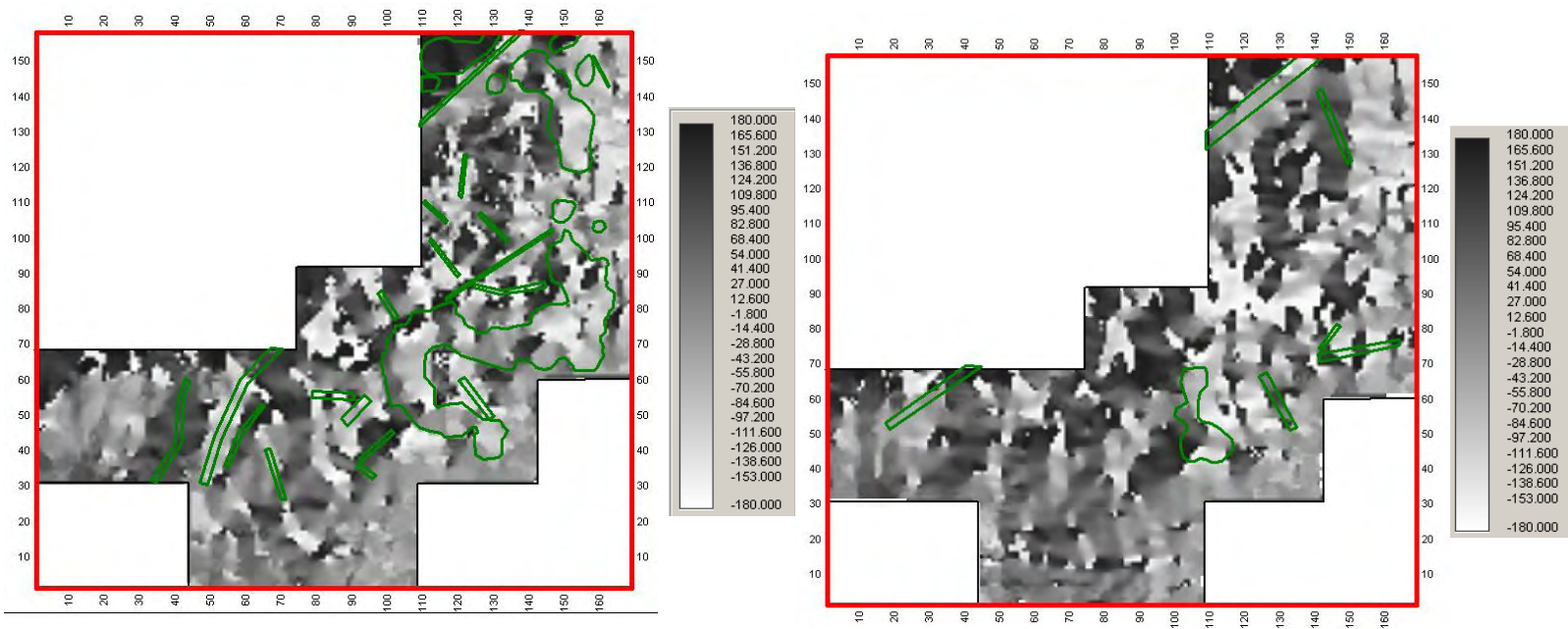


Figure 10: Dip Azimuth maps extracted from the Mississippian horizon(left) and Fort Scott horizon(right).

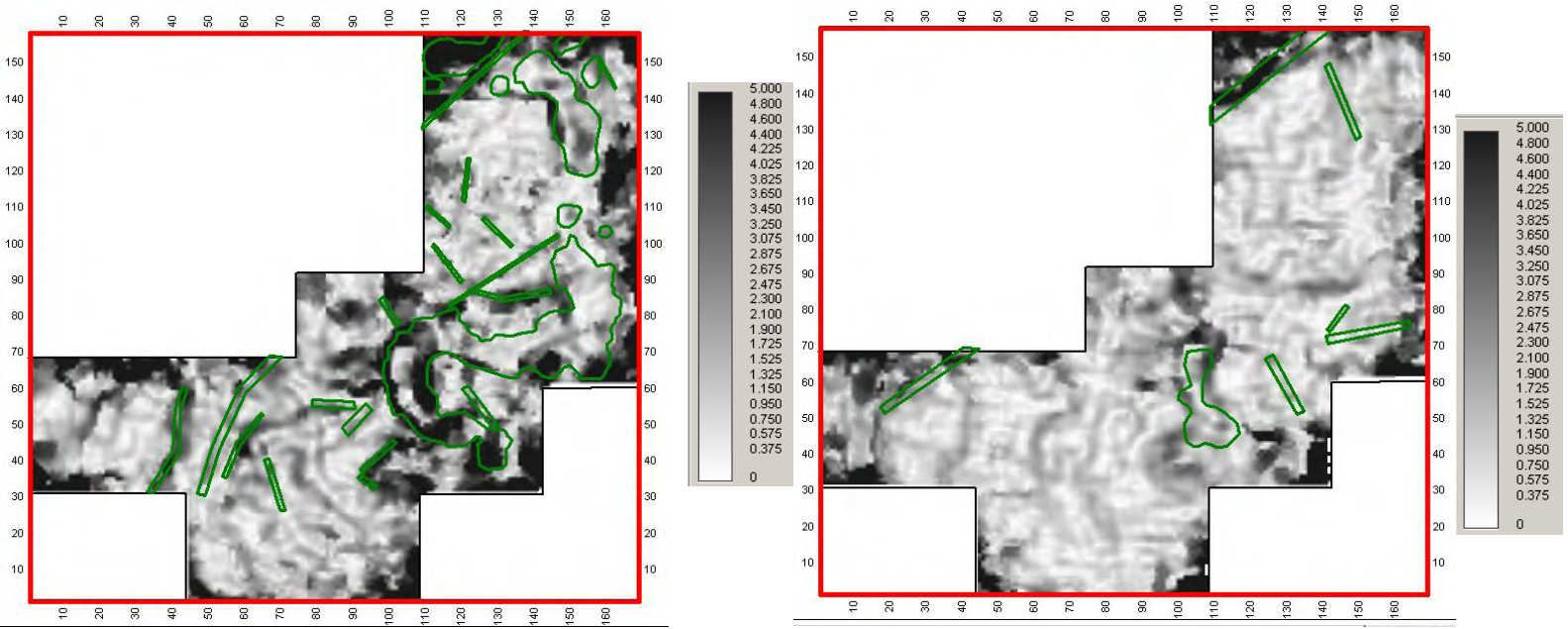


Figure 11: Dip magnitude maps extracted from the Mississippian horizon(left) and Fort Scott horizon(right).

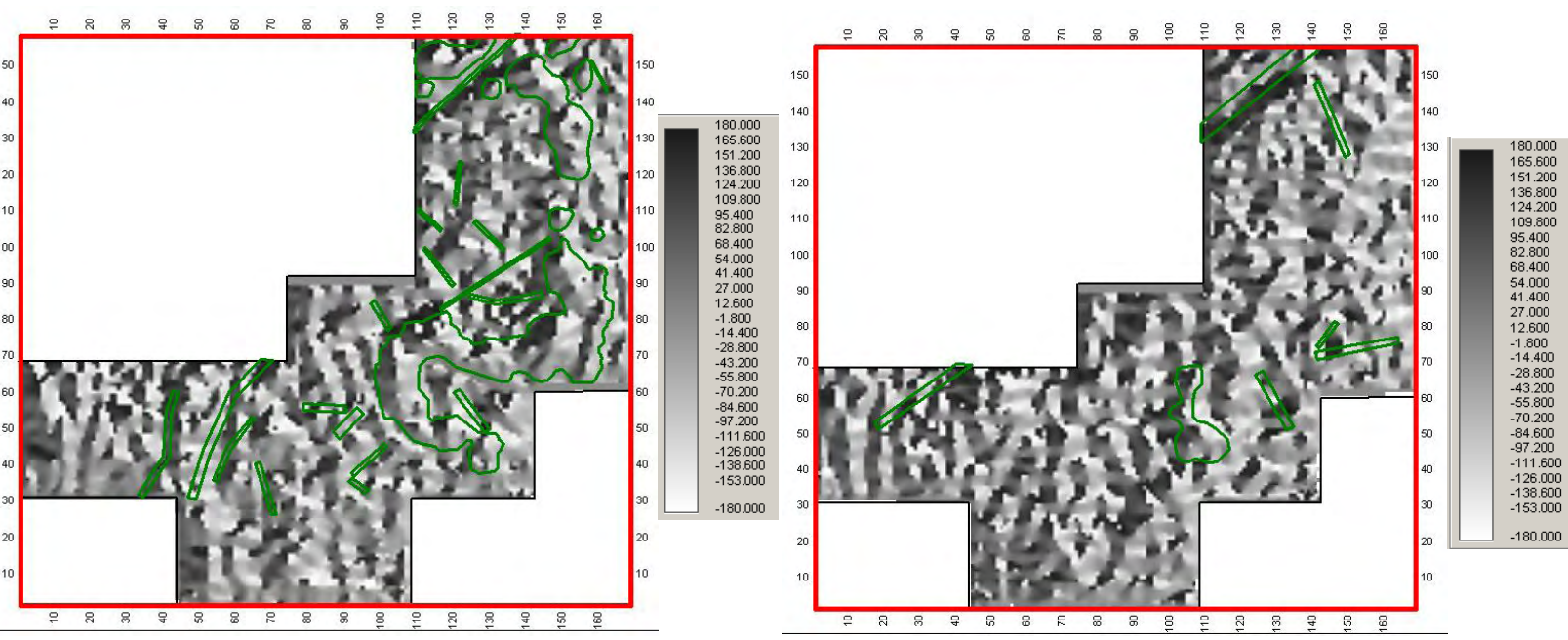


Figure 12: Gradient azimuth maps extracted from the Mississippian horizon(left) and Fort Scott horizon(right).

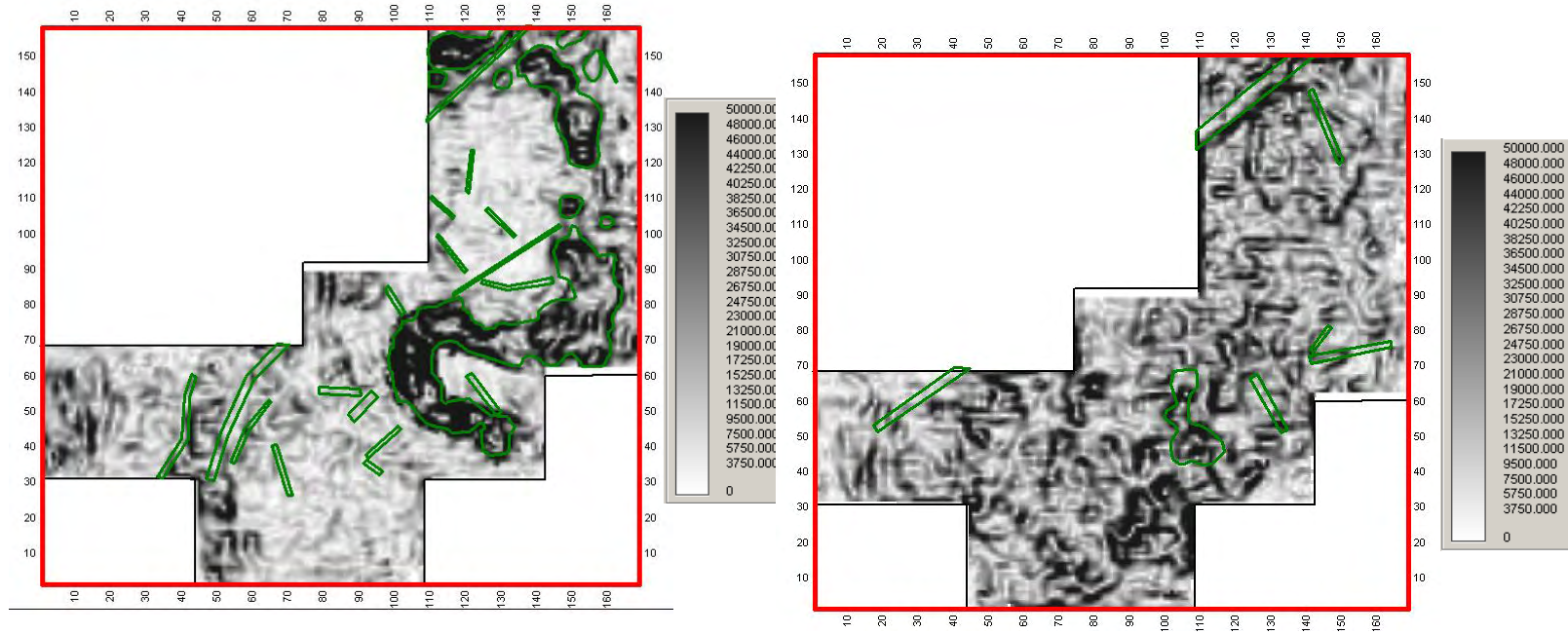


Figure 13: Gradient magnitude maps extracted from the Mississippian horizon(left) and Fort Scott horizon(right).

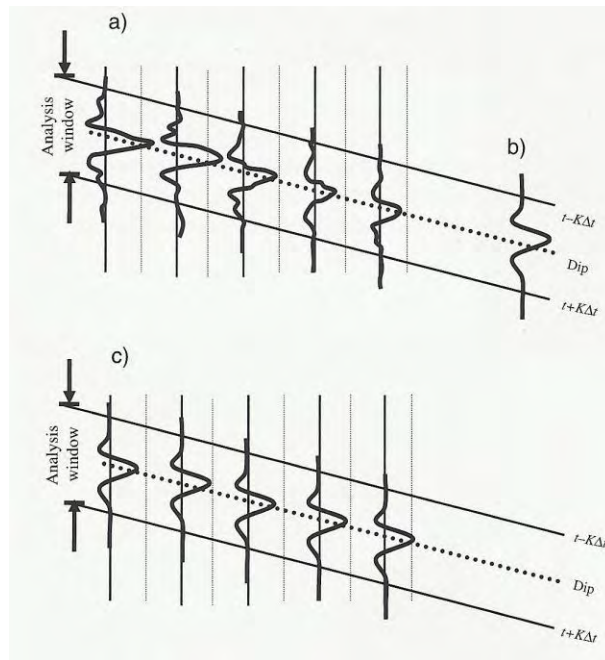


Figure 14: A diagram showing how semblance-based coherence is calculated. (a) Shows the input traces and the analysis window in which the energy will be calculated, (b) shows the calculated average trace, and (c) shows the traces replaced with the average trace. The semblance is the ratio of the energy

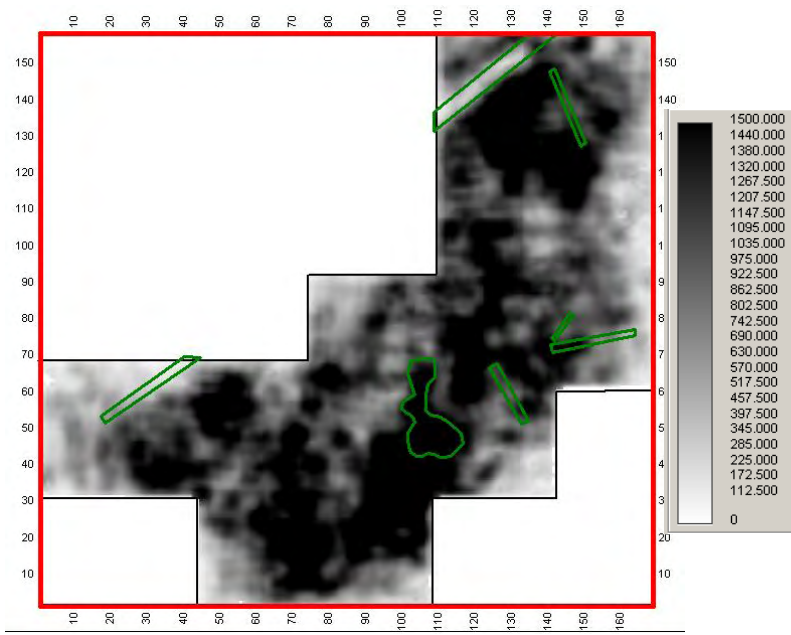
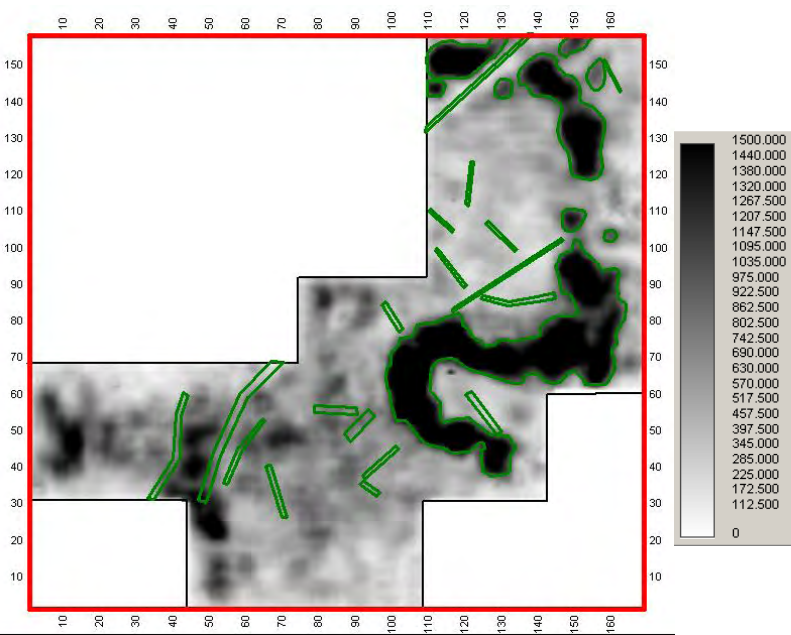


Figure 15 Total energy maps extracted from the Mississippian horizon(left) and Fort Scott horizon(right).

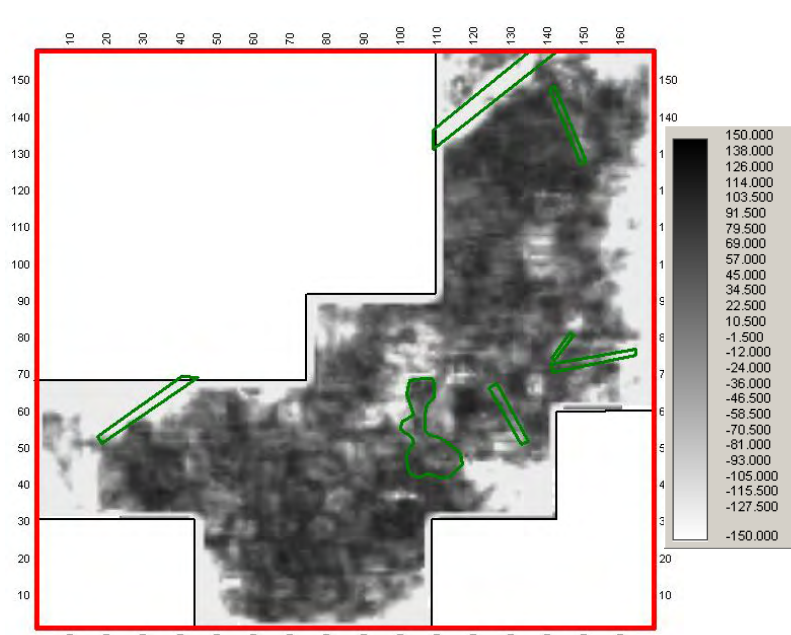
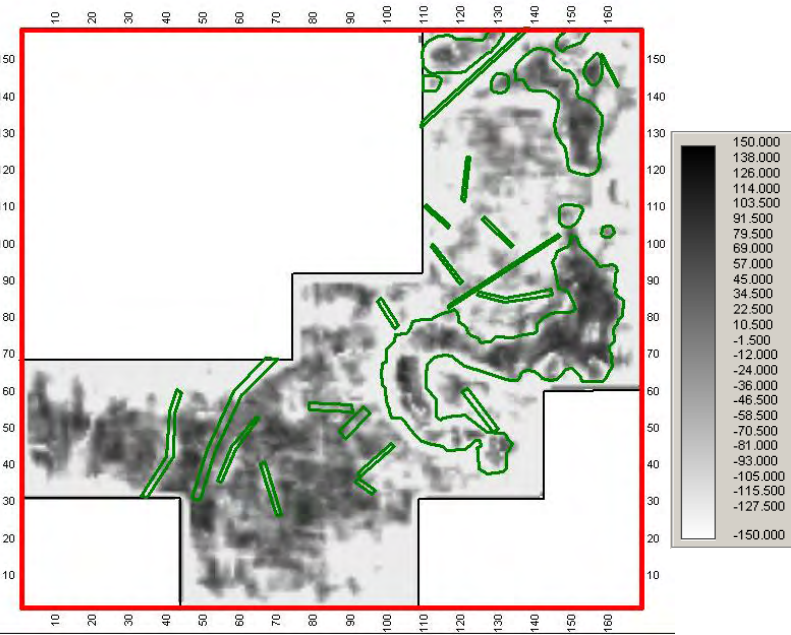


Figure 16: Energy ratio maps extracted from the Mississippian horizon(left) and Fort Scott horizon(right).

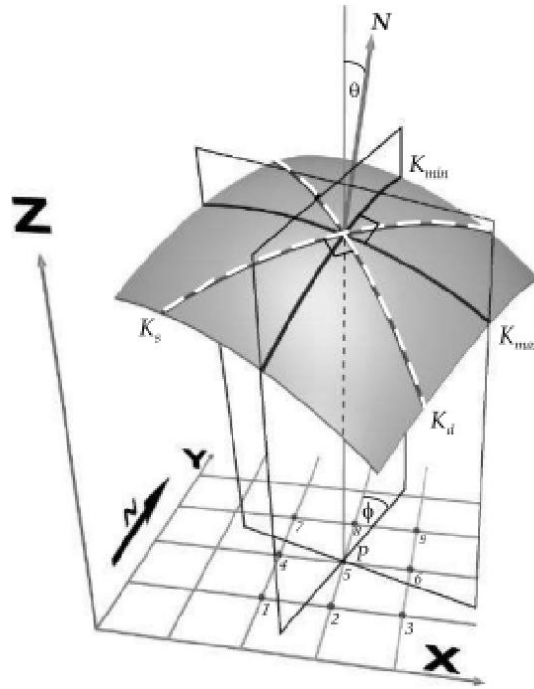


Figure 17: Diagram showing curvature naming conventions in 3D. X and y represent the map axes and z represents depth. N is the vector normal to the point P which makes an angle θ with the vertical. K_{\max} is the maximum curvature, K_{\min} is the minimum curvature, K_s is the strike curvature, and K_d is the dip curvature (Roberts, 2001).

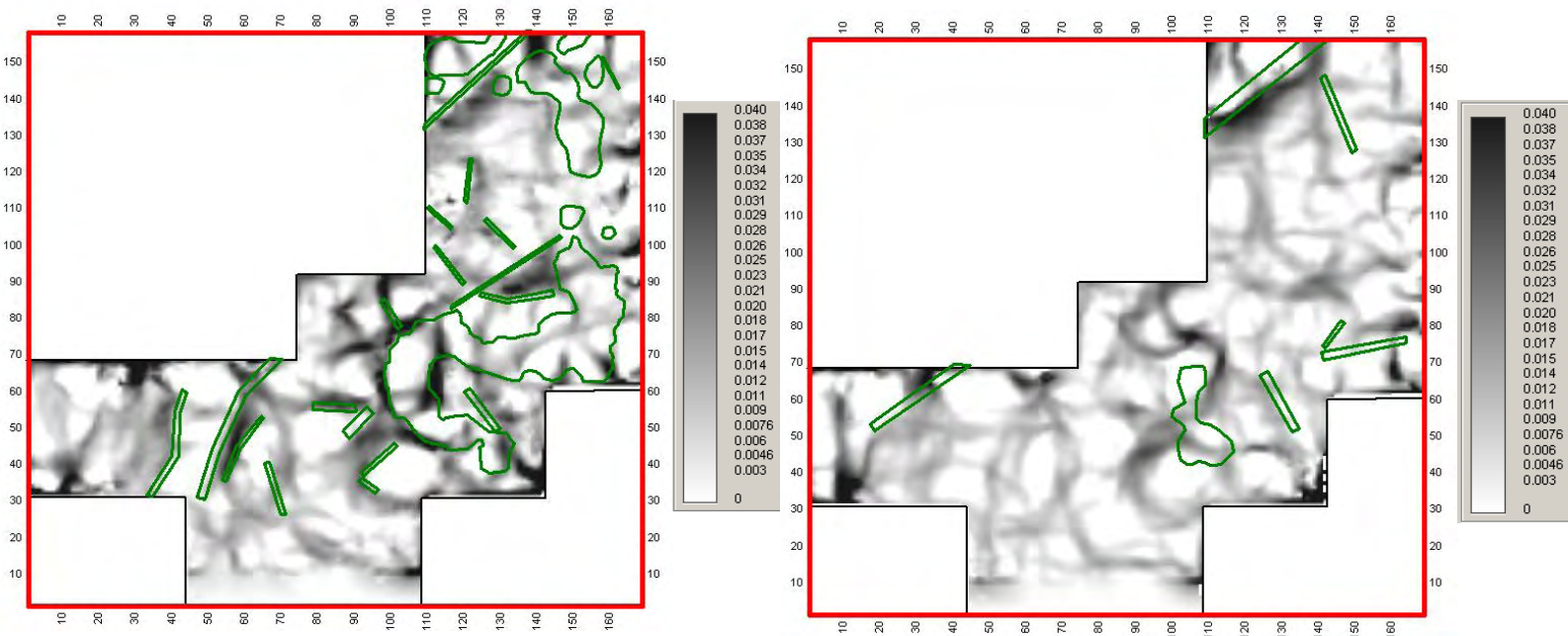


Figure 18: Positive curvature maps extracted from the Mississippian horizon(left) and Fort Scott horizon(right).

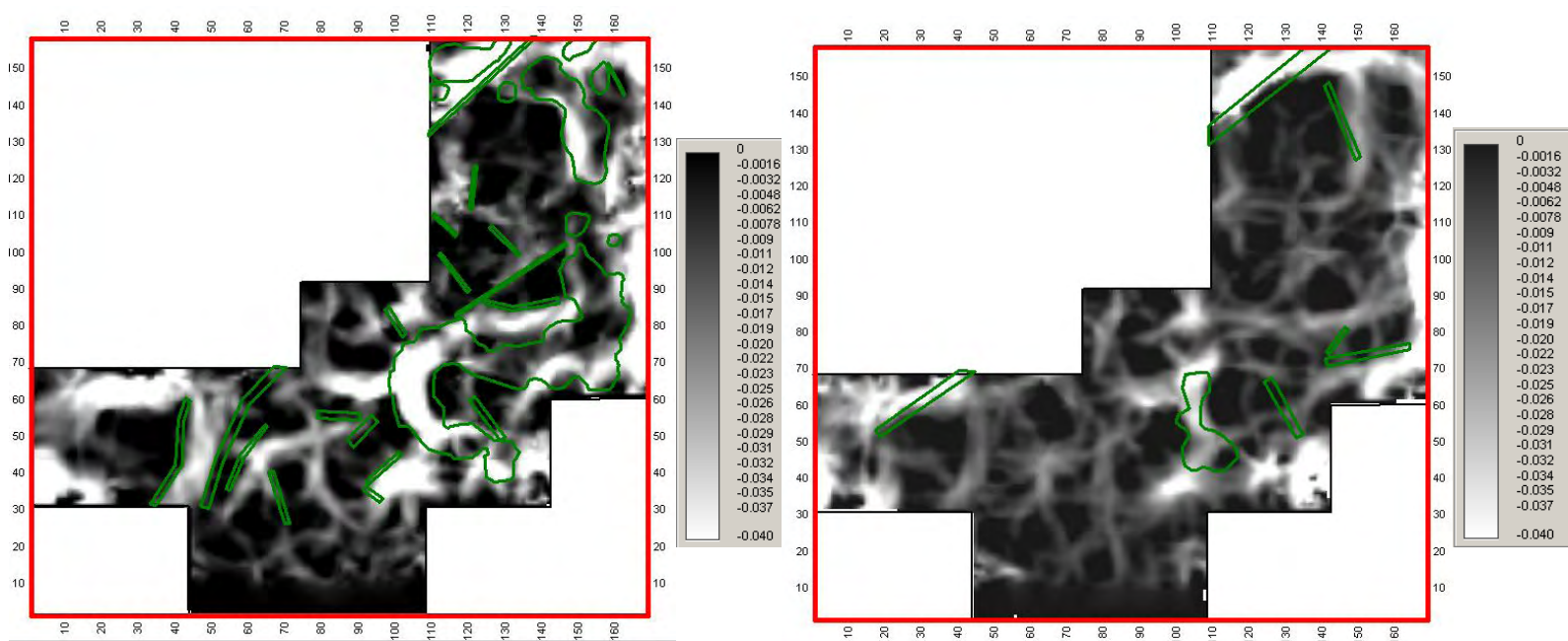


Figure 19: Negative curvature maps extracted from the Mississippian horizon(left) and Fort Scott horizon(right).

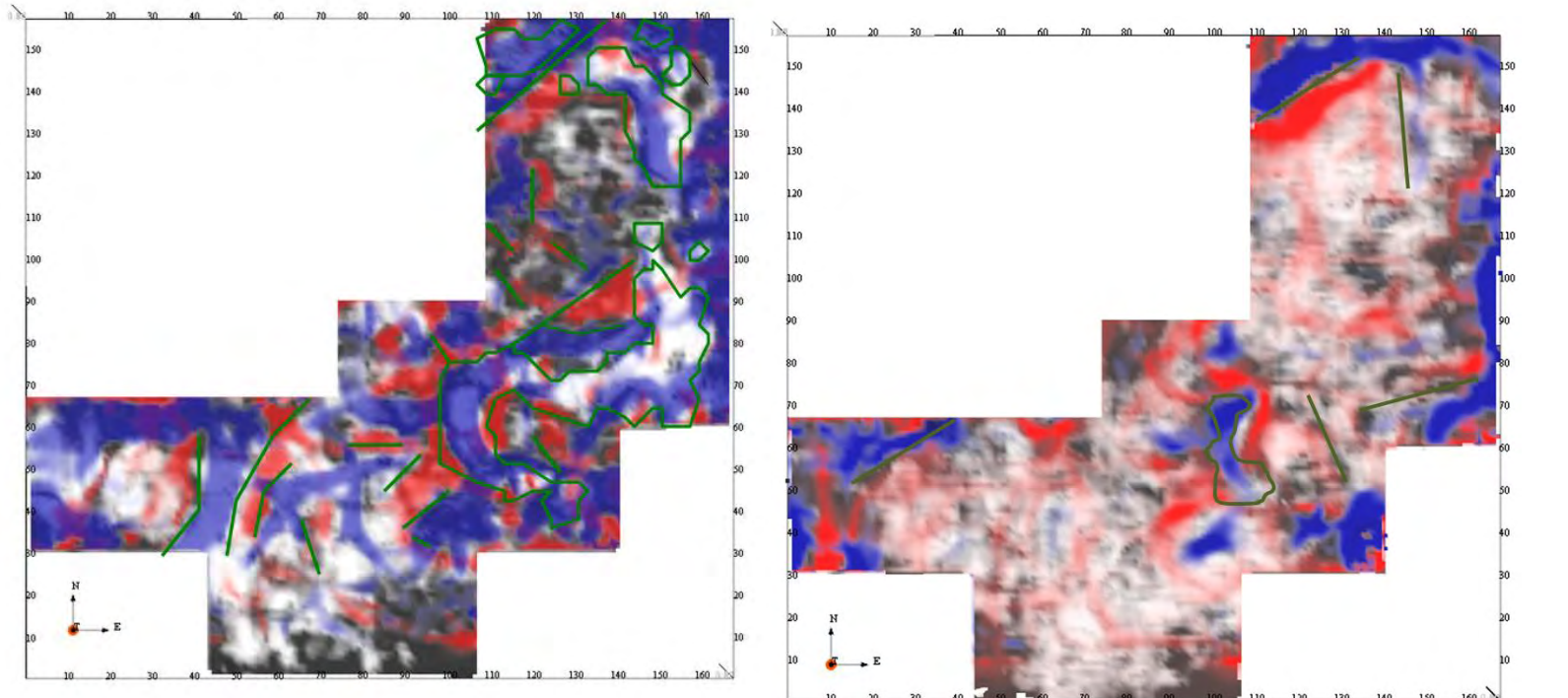


Figure 20: Energy ratio maps extracted from the Mississippian horizon(left) and Fort Scott horizon(right).

References

- Bahorich and Farmer 1995, 3-D seismic discontinuity for faults and stratigraphic features: The coherence cube: *The Leading Edge*, 14, no. 10, 1053-1058.
- Chopra, S., Marfurt, K., 2005, Seismic attributes -- A historical perspective, *Geophysics*, 70, 5, 3SO-28SO
- Chopra, S., Marfurt, K., 2007, Curvature attribute applications to 3D surface seismic data, *The Leading Edge*, 26, 404.
- Gerhard, L. C., 2004, A new look at an old petroleum province: Kansas Geological Survey, *Current Research in Earth Sciences*, 250, part 1, accessed April 16, 2009; <http://www.kgs.ku.edu/Current/2004/Gerhard/index.html>.
- Hilterman, F., and Bjorklund, T., 2007, Application of Cutting-Edge 3-D Seismic Attribute Technology to the Assessment of Geological Reservoirs for CO2 Sequestration, DOE October-December quarterly report.
- Merriam, D. F., 1963, *The Geologic History of Kansas*: Kansas Geological Survey Bulletin, 162, accessed April 14, 2009; <http://www.kgs.ku.edu/Publications/Bulletins/162/index.html>
- Moore, R.C., 1949, Divisions of the Pennsylvanian System in Kansas: Kansas Geological Survey Bulletin, 83, accessed April 14, 2009; <http://www.kgs.ku.edu/Publications/Bulletins/83/index.html>
- Nissen, S.E., Marfurt, K.J., and Carr, T.R., 2004, Identifying subtle fracture trends in the Mississippian Saline Aquifer Unit Using New 3-D Seismic Attributes: Kansas Geological Survey, Open-file Report 2004-56, <http://www.kgs.ku.edu/PRS/publication/2004/2004-56>.
- Rijks, E. J. H., and J. C. E. M., Jauffred, 1991, Attribute extraction: An important application in any detailed 3D interpretation study: *The Leading Edge*, 10, 11-19.
- Roberts, A., 2001, Curvature attributes and their application to 3D interpretation: *First Break*, 19.2, 85-99.
- Zeller, D. E., 1968, *The Stratigraphic Succession in Kansas, 1968*: Kansas Geological Survey Bulletin, 189, accessed January 29, 2009; <http://www.kgs.ku.edu/Publications/Bulletins/189>

Log Property Comparison to Seismic Amplitude
Analysis, Ness County, Kansas

Eric Swanson

December 2011

Log Property Comparison to Seismic Amplitude Analysis, Ness County, Kansas

Eric Swanson

Summary

The Mississippian formation in Dickman Field, Kansas, shows a bright amplitude horizon on seismic. Most wells penetrated the top of this formation, however not all wells have a full suite of logs. The goal is to determine if any log properties correlate with this increase or decrease in amplitude along the Mississippian horizon.

The first step was to map the top of the Mississippian Limestone. The map was generated by tying the wells to seismic with an accurate time depth chart by creating a synthetic using the Elmore 3 well. The horizon was then interpolated over the entire 3D by picking every 10th inline and cross line. The next step was to analyze all the wells log properties and pick the top of the Mississippian. Once this was complete the log property values for different logs were cross plotted against amplitude values at the well location. The last step was analyzing these cross plots and look for trends to correlate with petrophysical or geophysical properties.

Statement of problem and Objectives

Dickman Field located in central Kansas produces hydrocarbons from the Mississippian reservoir. The Mississippian in this area ranges from 100 to 300 feet thick. Most of the

wells in this study penetrated the top of this formation, with very few penetrating the entire Mississippian formation. The Mississippian formation has been studied extensively in the state of Kansas and surrounding areas because of its shallow nature and hydrocarbon production potential.

The main objective of this study was to try and tie log properties (i.e. gamma ray, resistivity, neutron, calculated porosity) to the bright amplitude at the top of the Mississippian unconformity. The process involved extracting both the amplitude data at the well locations and the petrophysical log data at the Mississippian formation depth and cross plotting the amplitude with the different log data to look for a trend. After careful analysis of the cross plots some trends were identified. Further research was then done to determine geologic/geophysical and petrophysical reasoning behind the trends and define why a trend exists based on knowledge of the field and reasoning found in research.

Background information

Dickman field is located in the northern half of Ness County in central western Kansas (figure 1). The field was discovered in 1962, and has produced 1.8 million barrels of oil to date (Kansas Geologic survey).

Goebel (1968) described extensively the geologic description of Mississippian rocks in western Kansas. Most of the research has been prompted by the large amounts of hydrocarbons present in the Mississippian rocks and it's important to better understand for future potential. Goebel described most of the rocks deposited during this time as carbonate-cherty and noncherty dolomite and limestone and dolomitic limestone. It was

noted in Rogers (2007) that the “precambrian, Ordovician, and Mississippian age rocks were exposed and truncated prior to regional Pennsylvanian transgression in most of western Kansas”. This exposure and transgression series caused irregular erosional surface also known as Karst. The regional dip of the Mississippian is approximately 14 ft/mi toward the southern boundary of Kansas Goebel (1968). Goebel also noted that most of the uplift of the western Kansas Mississippian surface occurred before the invasion of the Pennsylvanian seas. This study area sits just west of the central Kansas uplift as can be seen in (figure 2).

Research into seismic attributes correlation began in 2004 (University of Kansas center for Research, et al., 2009). Nissan et al. (2006) published a paper identifying fracture trends and the relationship of these fractures to karst features. In addition a study of the possibilities of carbon dioxide sequestration was done by Sullivan, et al., (2006). Most recent work has been done by Barber and Marfurt (2009) where they modeled the reservoir to determine whether the valley-shaped lineaments in the seismic data were a result of velocity “push down” effect or karstification. Malleswar and Marfurt (2011) additionally showed the relationship between seismic curvature and fractures identified from image logs.

The geology of the Mississippian is mostly interbedded sand, shale, and carbonates Moss (1932). In Dickman Field the Mississippian is mostly fractured porous and solution enhanced shelf carbonates (dolomites) (Liner et al., U. Houston). There is no significant faulting in the area and mostly the stratigraphy is flat except for a channel feature in the south east corner. Most of the production comes from porous Mississippian carbonates with structural closures. The elevation in the area is around 2400 to 2500 feet above sea

level. The Mississippian is about 4300 to 4400 depth which is about 1900 feet above sea level. The top of the Mississippian is karst surface where production also comes from sandstone reservoirs in the Lower Cherokee group deposited where the sub aerial karsting created low spots (Liner et al. U. Houston). The Lower Cherokee can be seen in type log in figure 3.

Through further research from (Liner et al., U. of Houston) it is found the seismic vertical resolution is 82.5' and the horizontal resolution is 165'. Also, the top of the Mississippian was determined to be a trough (most negative amplitude). Because amplitudes are an important part of this study a review of the processing parameters are included in Appendix A. The survey was reprocessed in 2007 by University of Houston with the intention of testing various attributes for the larger CO2 sequestration study (Liner et al., U. of Houston). The 3D dataset has 158 inlines and 169 crosslines with 82.5 feet interval spacing and covers 3.3 square miles. (Liner et al. U. Houston).

Methods

The first step was to go through and verify wells with logs and to analyze the petrophysical properties and pick the top of the Mississippian. This involved using a type log from the Califf study (figure 3) and creating several cross-sections in both the north-south direction and the east-west direction to verify the Mississippian top correlated across the field. (Figure 4) is an example of a north-south cross-section. Every well in the project was included in this part of the process. There were 140 wells in the project, (figure 5 shows the outline of seismic and all the wells) of which about 58 had well logs

in and around the seismic data area. Of those wells some were outside the 3D or lied close to the border that their tops where used in the cross-section, but were later dropped because it was felt that since the wells were on the edge of the seismic data set they lacked the full fold coverage and the amplitude values could give erroneous values the data. It was next determined that 24 wells were in the seismic area and contained good log data across the Mississippian.

Next step was to extract the log values. This was done by exporting the logs in .las format and importing them into excel. Once this was complete the values from the top of the Mississippian was taken and all data below that depth. In the event that the well was logged below the Mississippian the base depth of the Mississippian was used as the lower cutoff and no data below this point was included. After this a simple average over the logged Mississippian interval was taken for each log value. Figure 6 shows the spreadsheet where all the data was organized.

The Dickman 3D seismic project covers 4121 acres. Amplitude extraction was taken on two horizons. First the horizons were determined by tying the wells to seismic by creating an accurate time-depth chart. This was done by using Elmore 3 and creating a synthetic using SMT synPack module. Next it was determined that the best tie was a trough. The next step was to pick two horizons: 1) the trough that was determined when tying the data and 2)the peak just above. The peak just above was included to incorporate the Lower Cherokee sandstone values in the event of any karst infill. This will be explained in further detail in the results section (figure 7 is an example interpreted

crossline). The horizon interpretation was initially done by picking every 10th inline and cross line (figure 8 is an example every 10th inline-cross line picked). After this a picking interpreter in SMT (3D hunt) was used to fill in the remaining in lines and cross lines (figure 9 shows the interpreted horizon for the trough). Once this was complete a grid was made of each horizon extracting the amplitude values (figures 10 and 11). The last step of the amplitude extraction was to record the amplitude value from the grid at each well location. To verify that the gridded amplitude values would represent an accurate amplitude value a test was done on two wells that involved extracting the value of the 3 nearest traces in inline and cross line direction by using the cursor recorded the value of the amplitude at each of these traces. Averaging these 6 traces proved to have a close value of the gridded amplitude within 10%.

The next step was to cross plot each of the amplitudes at the well locations with the different log values for all the wells in the project area and analyze the results.

Results

The results for the resistivity cross plot showed a general increase in amplitude with decreasing resistivity values for both peak and trough (figures 12 and 13). Resistivity measures how resistive a formation and its fluid is, in other words it measures the resistance to passage of an electric current Rider (2000). Most rock materials are insulators, while their enclosed fluids have conductive properties and for water saturation is tied to salinity (resistivity increases with more saline water). Hydrocarbons are

infinitely resistive Rider (2000). Some other notes on resistivity: 1) as porosity increases resistivity will decrease 2) hydrocarbon formation resistivity will be higher 3) in tight rock resistivity will be higher. In conclusion in areas where we have higher amplitude we tend to have lower resistivity which could mean we have higher porosity and may be tied to water saturation.

The results on the neutron-amp cross plot showed that values decreased slightly with increasing peak amplitude for the peak (figure 14) and no real trend for the trough (i.e. values for the neutron properties averaged flat over the different trough values) (figure 15). Neutron log values measure porosity and are indicators of hydrocarbon richness. Neutron logs also are more accurate in tighter rocks. The data for the peak-amplitude cross plot showed a decreasing neutron with increasing peak. This could mean where we have higher amplitudes we have greater presence of hydrocarbons or water. Water and oil can be difficult to separate with just this cross plot method, but this could be an indication of water saturation. The lower neutron count could also result from higher porosity which agrees with the resistivity (but these are based on the presence of fluids) and does not agree with the calculated porosity log which should be calibrated to lithology.

The Gamma values on the cross plot had a slight trend of decreasing in gamma value with increasing amplitude values for both the trough and the peak (figures 16 and 17 respectively). Gamma measures the radioactivity of rock. Most often gamma logs are used to quantitatively derive shale volume Rider (2000). Gamma ray also decreases in

the presence of carbonates because of the general lack of shales. This decrease in gamma could be a result of the carbonates in the Mississippian along with the harder dense limestone.

There was also a calculated porosity log available on most wells. When this value was cross plotted against amplitude the results showed a decrease in porosity with increasing amplitude for both peak and trough (figures 18 and 19). This could possibly result from less porous more dense limestone causing an increase in reflection impedance.

.

Conclusions

There were some trends in the data; although most cross plots resulted in poor correlation and just a general trend. Some of this was probably the result of not having very many wells for most cross plots. However some trends were noticeable. The resistivity showed a decrease in value with increasing amplitude. The gamma values showed a slight increase in amplitude with decrease gamma values. The neutron log showed a very small trend of decreasing neutron values with increasing peak amplitude. No trend was found for the neutron trough cross plot. There was also a calculated porosity which showed a decrease in porosity with increasing peak.

Watney et al. (2001) studied characteristics of chat in south central Kansas nearby field to the Dickman field. Part of the conclusion was “Irreducible water, bound in the chert microporosity, greatly diminishes the resistivity log response and leads to high water saturations in zones that produce large amounts of oil and little water”. Although we

don't have production values for these individual wells high water saturation could be a reason for the change in resistivity.

The accumulation of this data has a few additional results. The Lower Cherokee Sandstone is a thin bed approximately 20' thick. Rogers (2006) while describing Garfield conglomerate pool, in Pawnee county Kansas (a similar reservoir to adjacent Ness county) described the sand "origin and distribution of valley-fill sand-stone deposits, which produce oil from topographic and or karst depressions carved into Mississippian cherty limestone at the pre-pennsylvanian unconformity". This karstic infill sandstone could be having an effect on the amplitudes, although it's below the seismic resolution.

Additionally the results may have a strong tie to water saturation. The decrease in resistivity could mean higher porosity with high water saturation. The decrease in Gamma ray is probably a result from the less shaley carbontes found in the Mississippian. Also, the lower neutron is an indicator of increase pore fluids whether it be from hydrocarbons or water.

After further research it was determined that the geology of the top of the Mississippian was very complex. Many studies were done throughout Kansas and into the play in Oklahoma. In the southern part of Kansas the top of the Mississippian formation contains what's called chat fields. "Chat" is an informal name for high porosity, low resistivity producing chert reservoirs in the mid-continent where porosities can range from 30-50% Watney et al., (2001). Investigating if there was a way to discern chert with the logs available led to the conclusion that since sandstone, quartz, and chert all have the same chemical makeup they will show a similar response on the logs.

Future work could be incorporate production data and or water saturation calculations.

At the time of this study there were only 8 wells with production data available. Six of these wells were in an area that was considered good seismic data. Further production data should be available and could be incorporated into this study by further extending the petrophysics analysis of each well log.

References

Barber R., Marfurt K. Attribute Delineation of Karst- Calibration via elastic Wave-Equation Modeling: 2009 Ann. Internati. Mtg., Soc. Expl. Geophys., Expanded Abstracts, 2627-2631

Barber R., Marfurt K., Attribute Delineation of Karst – Calibration via Elastic Wave-Equation Modeling: 2009 SEG Houston International Exposition and annual Meeting

Brown A., Interpretation of Three-Dimensional Seismic Data: 1999 Oklahoma: The American Association of Petroleum Geologist and The Society of Exploration Geophysics

Califf J., Integrated Depth Mapping of the Stone Corral from 3D Seismic and Well control in Dickman Field, Ness County, Kansas: 2010 University of Houston

Franseen, E. K., T. R. Carr, W. J. Guy, and D. S Beaty, 1998, Significance of depositional and early diagenetic controls on architecture of a Karstic-Overprinted Mississippian (Osagian) reservoir, Schaben Field, Ness County, Kansas: Presented at the AAPG Annual Meeting.

Goebel E., Mississippian Rocks of western Kansas: 1968 American Association of Petroleum Geologist Bulletin v. 52, No. 9, p. 1732-1778.

Kansas Geologic survey: <http://www.kgs.ku.edu>

Liner et al. U. of Houston

Malleswar Y., Marfurt K., Relation between seismic curvature and fracture identification from image logs – application to the Mississippian reservoirs of Oklahoma, USA

Other References

Nissen S., Carr T., Marfurt K., Using New 3-D Seismic Attributes to Identify Subtle Fracture Trends in Mid-Continent Mississippian Carbonate reservoirs: Dickman Field, Kansas: 2006 Search and Discover article #40189

Nissen, S. E., T. R. Carr, and K. J. Marfurt, 2006, Using New 3-D Seismic attributes to identify subtle fracture trends in Mid-Continent Mississippian carbonate reservoirs: Dickman Field, Kansas, Search and Discovery, Article #40189.

Nissen, S. E., K. J. Marfurt, and T. R. Carr, 2004, Identifying Subtle Fracture Trends in the Mississippian Saline Aquifer Unit Using New 3-D Seismic Attributes: Kansas Geological Survey, Open-file Report 2004-56.

Rider M., The Geological Interpretation of Well Logs: 2006 Scotland: Rider-French Consulting Ltd.

Rogers J., New Reservoir model from an old oil field: Garfield conglomerate pool,
Pawnee County, Kansas: 2007 AAPG Bulletin, V. 91, No. 10, p. 1349-1365

Schoole P., Bebout D., Moore C., Carbonate Depositional Environments: 1998
Oklahoma: The American Association of Petroleum Geologist

Watney, W., W. Guy, and A. Byrnes, 2001, Characterization of Mississippian Osage
Chat in South-Central Kansas, AAPG Bulletin, v. 85, no. 1, p. 85-113

10. Iteration 1 velocity/mute analysis and application
11. Surface-consistent automatic statics 200-1000 ms statics gate
12. Iteration 2 velocity/mute analysis and application
13. Surface-consistent automatic statics 150-1050 ms statics gate
14. Final velocity/mute/scale analysis and application
15. CDP-consistent trim statics 4ms max stat
16. Bandpass filter 20/18-128/72 Hz/DM
17. Time variant scaling windows
18. Common depth point stack
19. Spectral enhancement 20-128 Hz
20. Post stack noise suppression FXY Decon
21. Fourier trace interpolation 110 ft xline interval to 82.5 ft
22. 3D FD migration 95% of RMS velocity field
23. Spectral enhancement 20-128 Hz
24. Bandpass Filter 20/24-120-72 Hz/DB
25. Trace balance time variant scaling windows

Acquisition details:

1. Date Recorded.....11/2001
2. Crew.....Lockhart Geophysical
3. Source Type.....Vibroseis

4. Sample Rate.....2 ms
5. Record End Time.....2 seconds
6. Receiver Interval.....220 ft
7. Receiver Line Interval.....660 ft
8. Shot Interval.....65 ft
9. Shot Line Interval.....880
10. Sweep.....20-128 Hz 12 sec 3DB/OCT
11. Instruments.....GDAPS
12. Format.....SEGY
13. Number of Data Channels.....324 MAX

Images

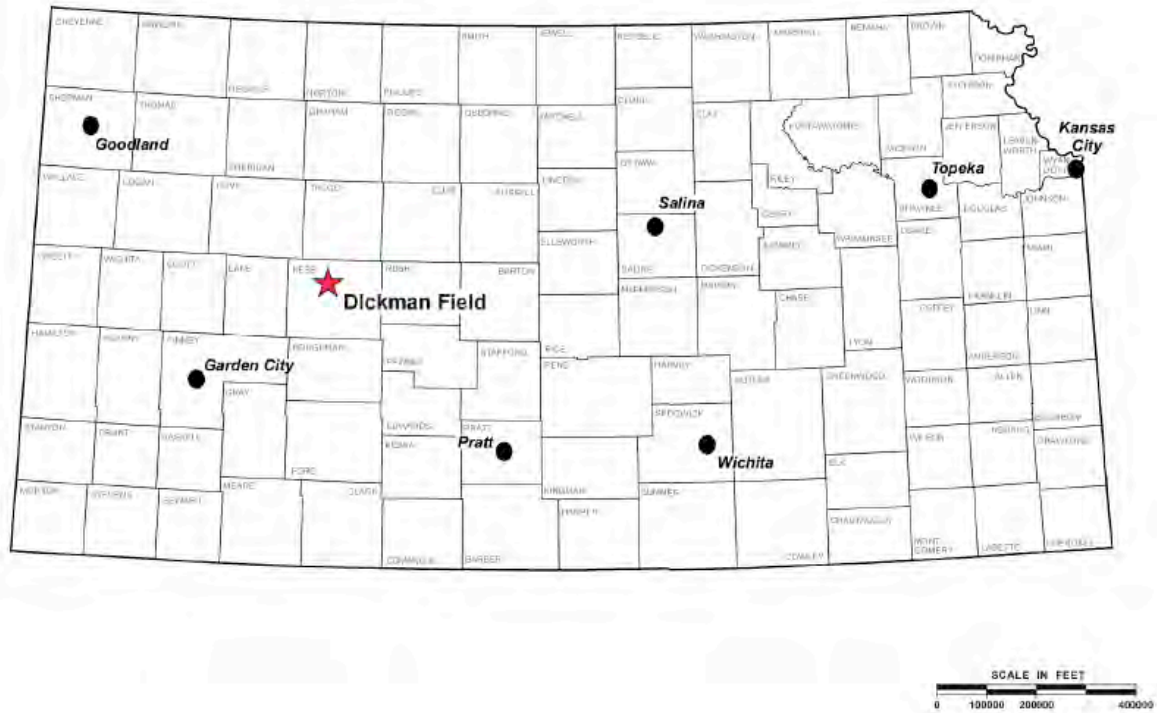


Figure 1: Field location of Dickman Field, Ness County, Kansas

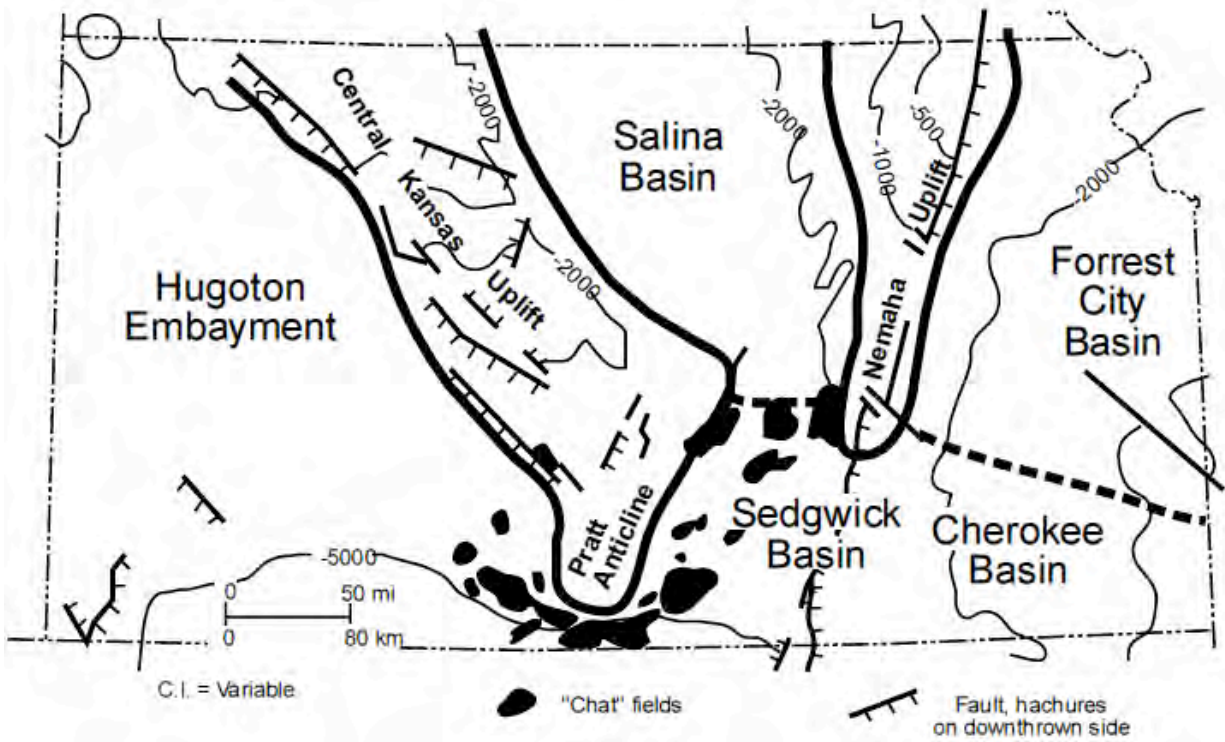


Figure 2: showing regional tectonic elements of south-central Kansas. (Montgomery et al. 1998)

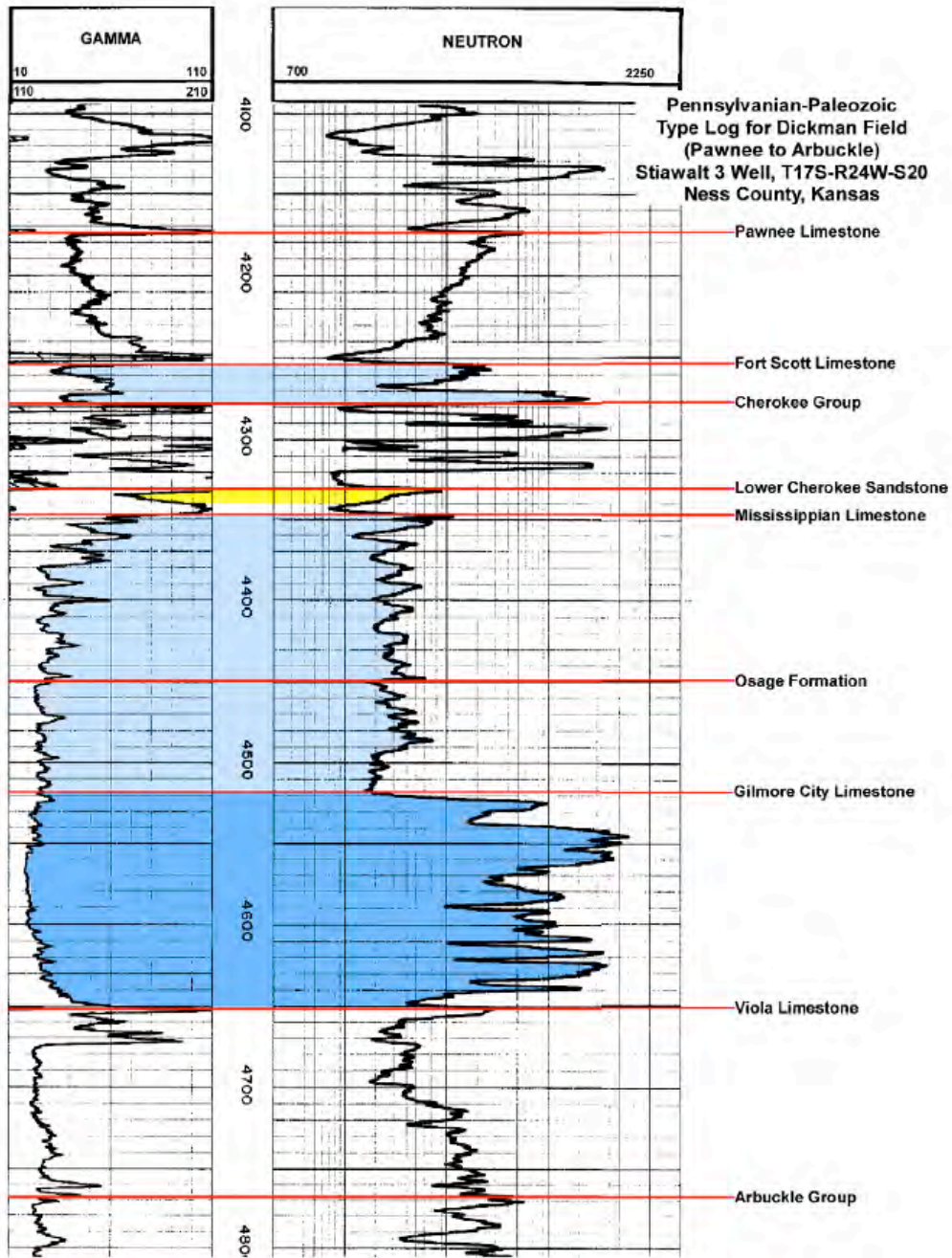


Figure 3: Type log showing the Mississippian Limestone

Arbitrary cross section

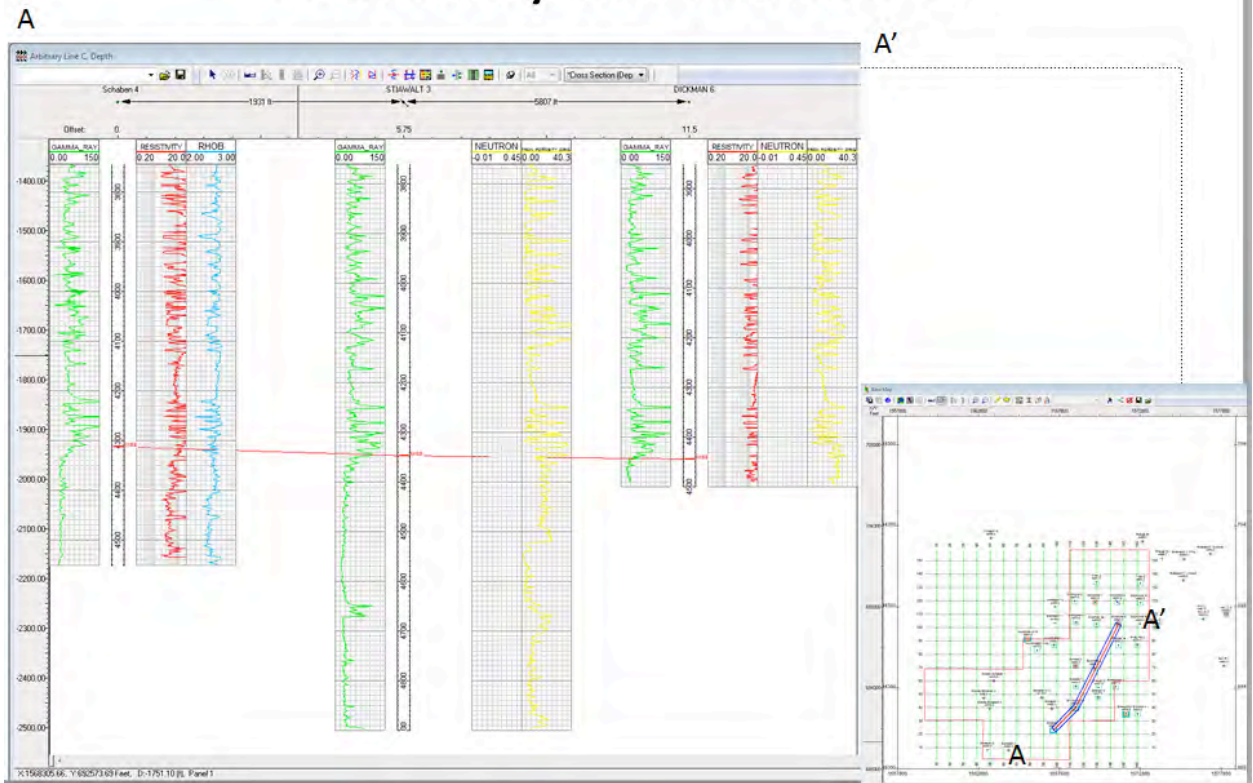


Figure 4 Cross section

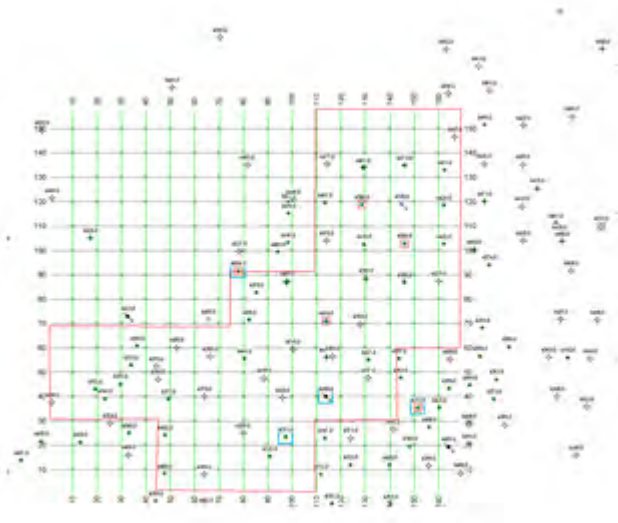


Figure 5: Outline of project area showing red outline of seismic data

well lists with taps																		
A	B	C	D	E	F	G	H	I	J	K	L	M	N	O	P	Q	R	S
1	Well name	UWI	Miss-Eric	Total depth	into Miss	log	amp-trough	amp peak	gamma	res	neu	sonic	por	cond	vel	vel_s	rhob	
2	DICKMAN 'A' 1	15-135-23724	4404.8	4422	17.2	y	-0.81	0.91	28.8495	20.68	354.607							
3	DICKMAN 'A' 2	15-135-23753	4419	4426	7	y	-0.97	0.59	32.984	26.82668	955							
4	DICKMAN 1	15-135-00174	4428	4500	72	y	-0.41	0.38	20.50977			65.312	15.107	115.3441				
5	Dickman 3a	15-135-30406	4389	4409	20	y	-0.25	0.02	38.89994		1046.489		17.657					
6	DICKMAN 4	15-135-90416	4460	4530	70	y	-0.56	0.42	47.27621		1268.3		17.54491					
7	DICKMAN 6	15-135-21256	4445	4500	55	y	-0.36	0.15	24.0158	25.06682	779.78		15.401		14513.4			
8	ELMORE 2	15-135-21468	4479.6	4501	23.4	y	-0.65	1.44	37.96481	4.99964	1111.083		20.70693					
9	Elmore 3	15-135-23755	4412	4464	52	y	-1	1.3	12.63	19.967	953.149		13.693		14974.77	14908.87		
10	HUMPHREY 3-18	15-135-24106	4359	4370	11	y	-0.42	0.64	29.81	8.1366	237.0618		22.8					
11	Mildred Schaben 3	15-135-22237	4346	4375	29	y	-1.15	0.93	21.865	12.83	903.2219							
12	Mildred Schaben 4	15-135-24189	4360	4390	30	y	-1.42	1.13	22.62059	8.967	276.89							
13	pHELPS 2	15-135-21326	4477			y	-1.28	0.91	29.09582	2.150926	1164.369		15.45					
14	Phelps 1a	15-135-21262	4452	4500	48	y	-1.23	0.93	14.6099	12.546	1355.36		14.66					
15	Schaben 1	15-135-21269	4381	4420	39	y	-0.71	0.96			1125.58							
16	Schaben 2	15-135-21257	4382.7	4400	17.3	y	-0.81	0.57	35.93656		1711.031							
17	Schaben 3	15-135-21378	4328			y	-0.81	0.44	38.027		1051.511							
18	Schaben 4	15-135-21452	4312	4551	239	y	-0.96	0.5	41.904	9.33							2.566465	
19	Schaben C 2	15-135-21892	4355	4418	63	y	-1.23	0.48	28.51597	8.6133	750.321							
20	Stewart 1	15-135-21393	4386	4433	47	y	-0.79	0.15	40.8738		936.748		20.798					
21	Stewart 2	15-135-21488	4368	4427	59	y	-0.82	-0.02	25.67		1102.241		22.108					
22	STIAWALT 3	15-135-21501	4347.9	4900	552.1	y	-0.9	0.14	38.748		1152.407		18.959					
23	Stewart 4	15-135-21646	4382	4437	55	y	-1	0.64	24.888		1272.717		20.518					
24	Tilley 2	15-135-27495	4442	4461	19	y	-0.054	0.34	12.78336									
25	Tilley 5	15-135-23869	4436	4451	15	y	-0.78	0.48	26.95582	18.3417	1206.547		19.33607					

Figure 6: Spreadsheet showing data collected

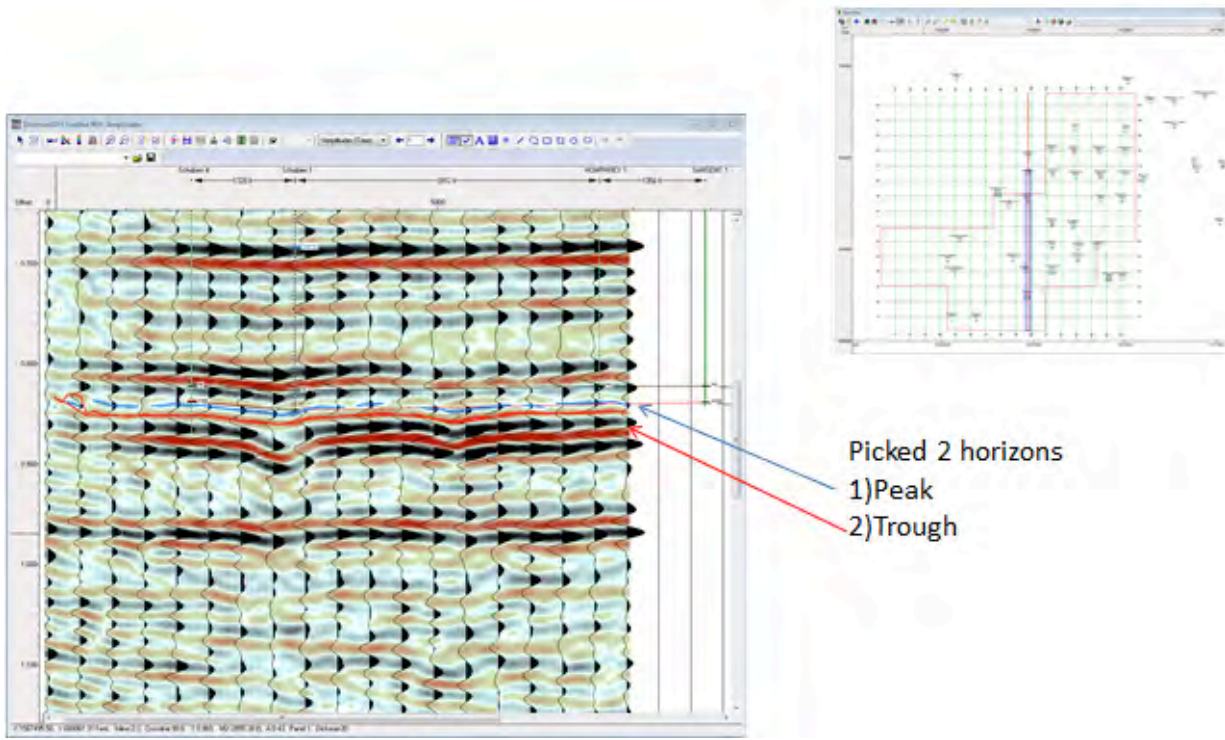


Figure 7: X-line 98 showing the peak and trough horizon pick for the top of the Mississippian

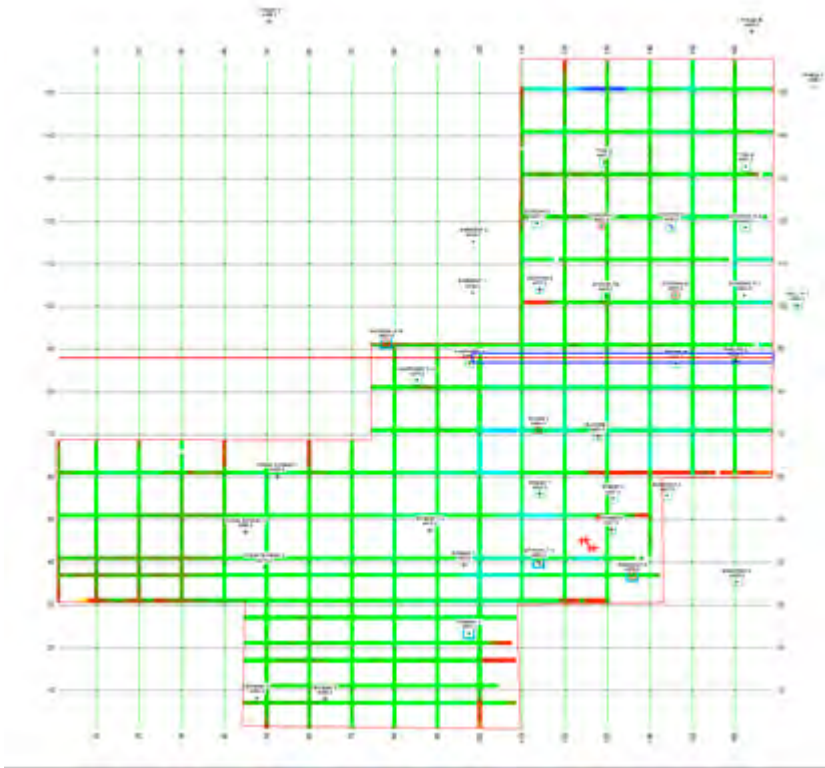


Figure 8: Every 10th inline and cross line picked on survey

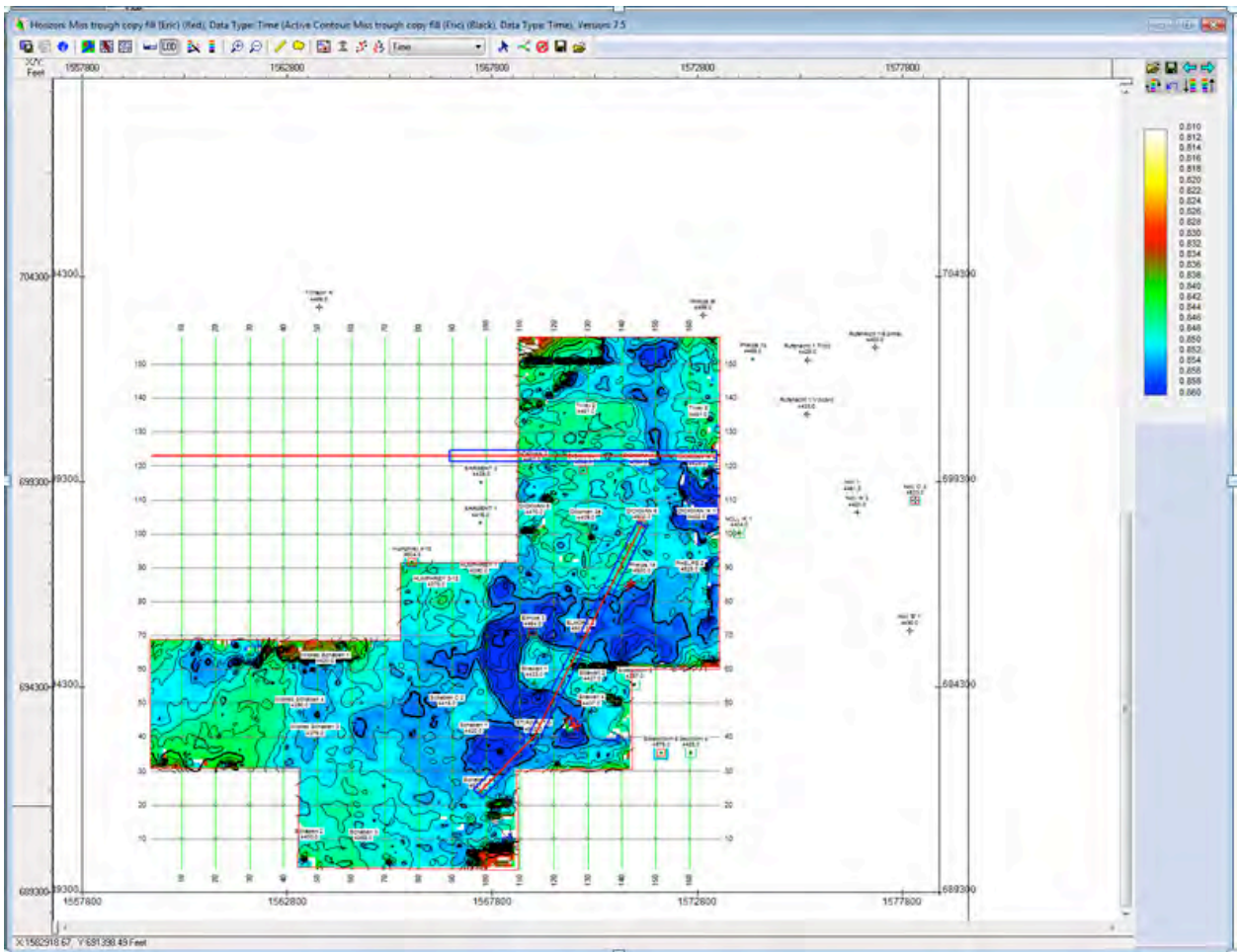


Figure 9 Structure map of Mississippi

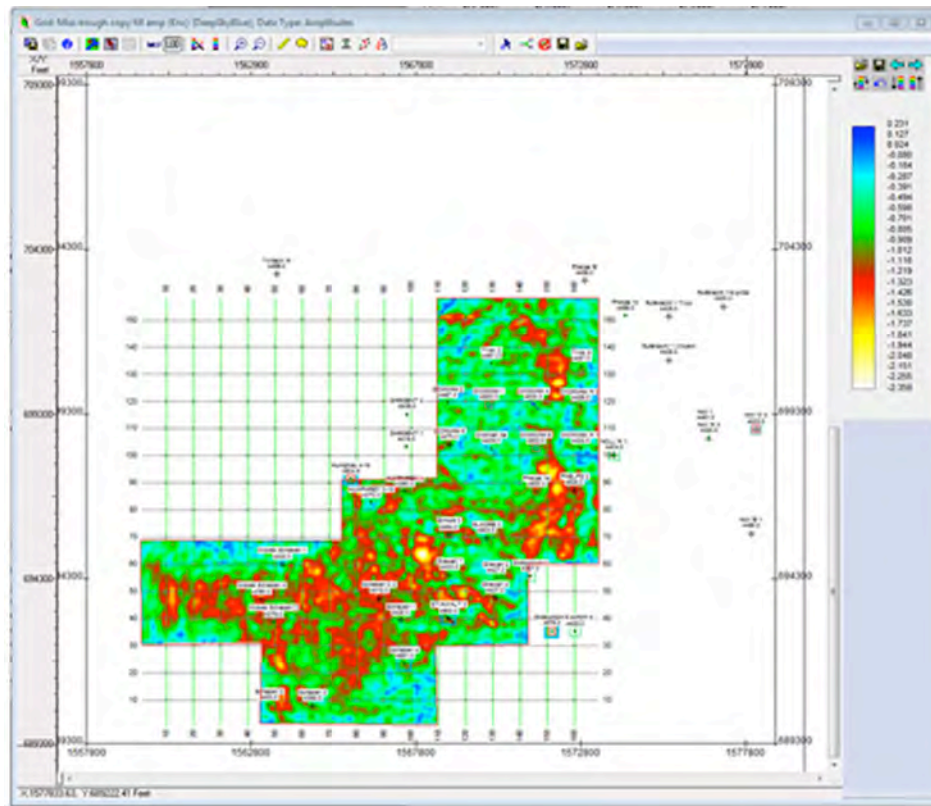


Figure 11: Amplitude map of trough

Peak vs resistivity

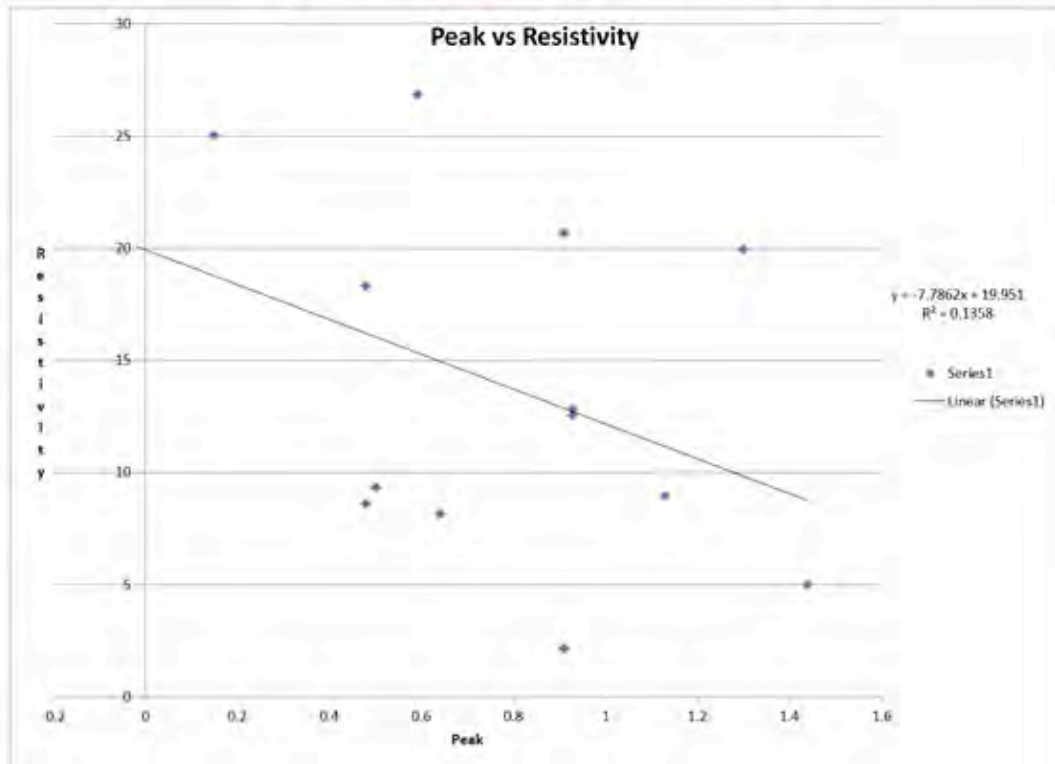


Figure 12: Peak vs Resistivity

Trough vs resistivity

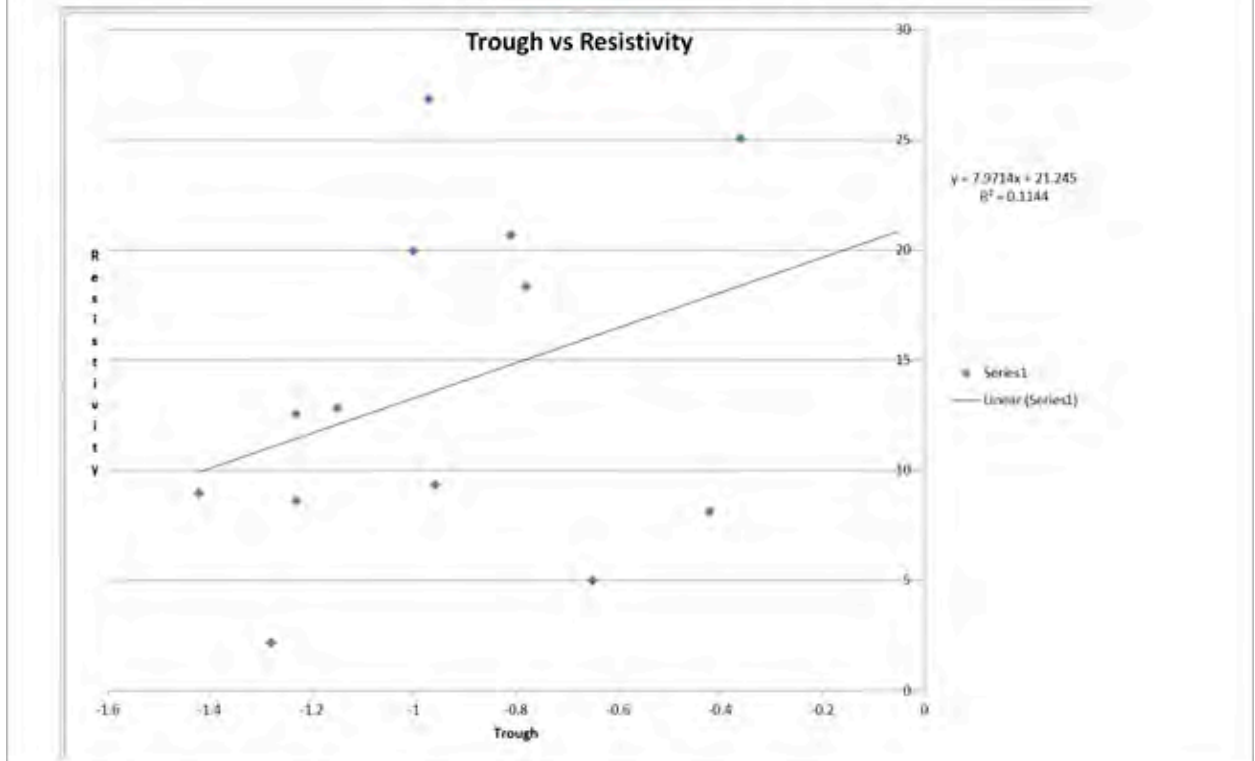


Figure 13: Trough vs Resistivity

Peak vs neutron

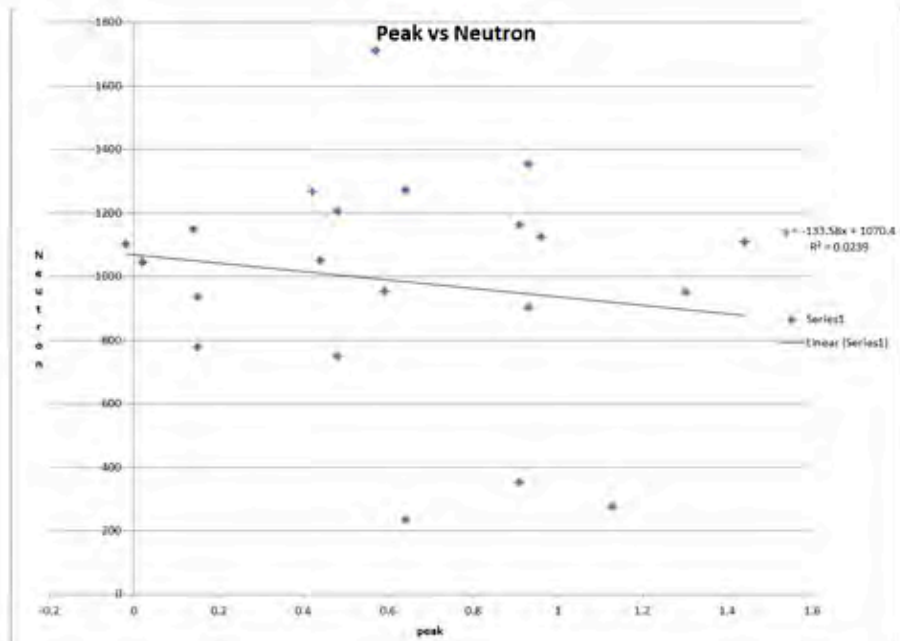


Figure 14: Peak vs Neutron

Trough vs neutron

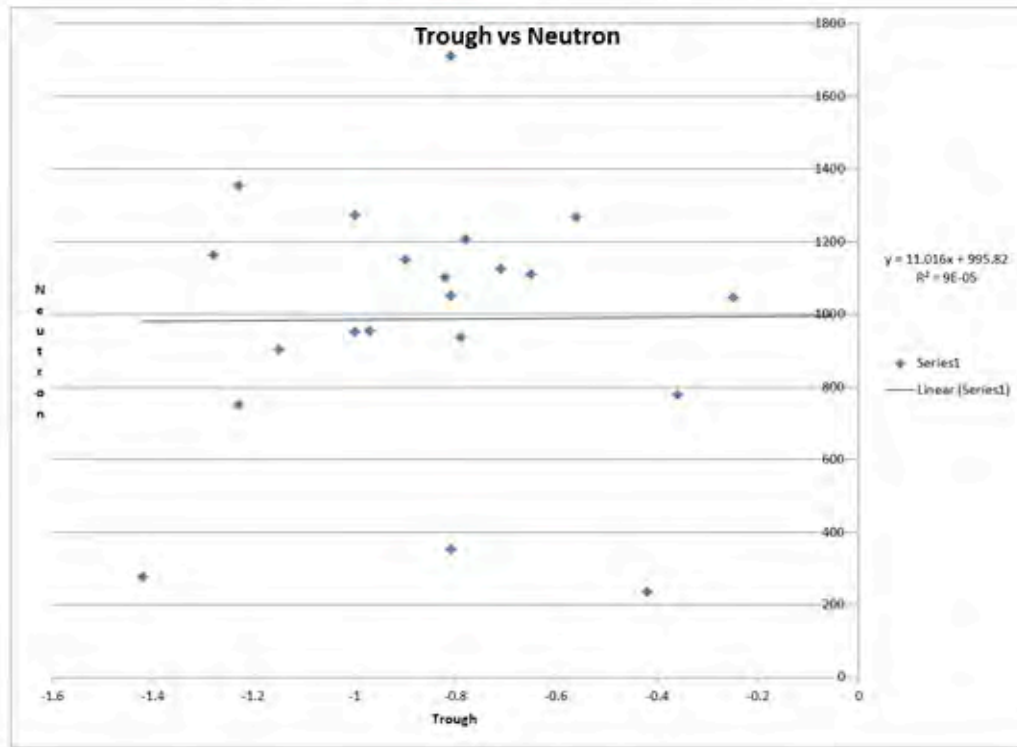


Figure 15: Trough vs Neutron

Peak vs gamma

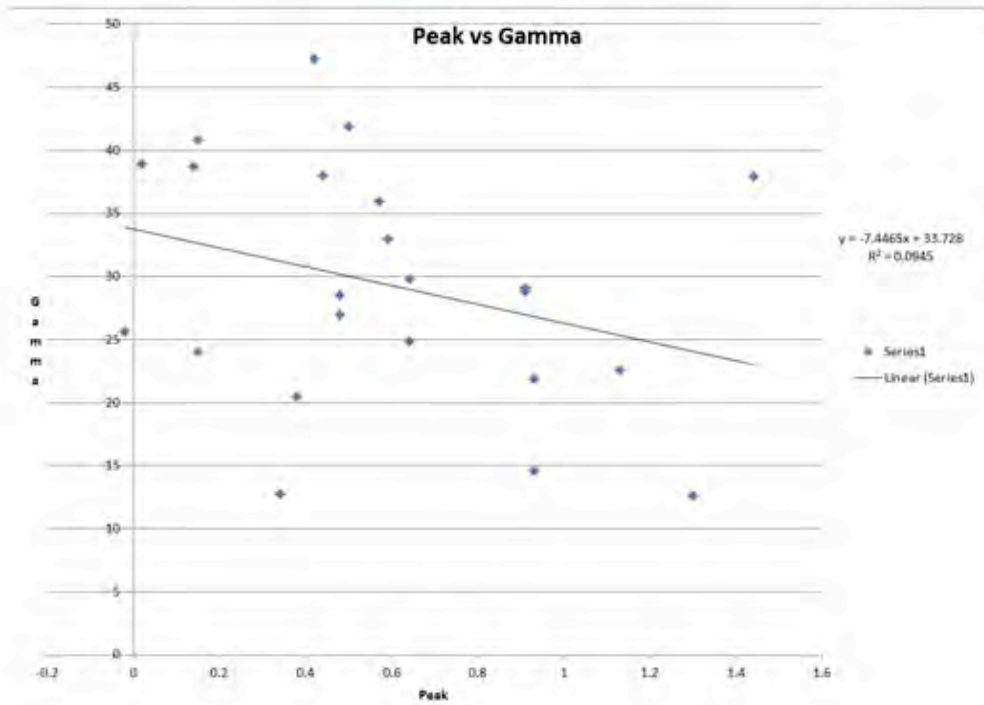


Figure 16: Peak vs Gamma

Trough vs gamma

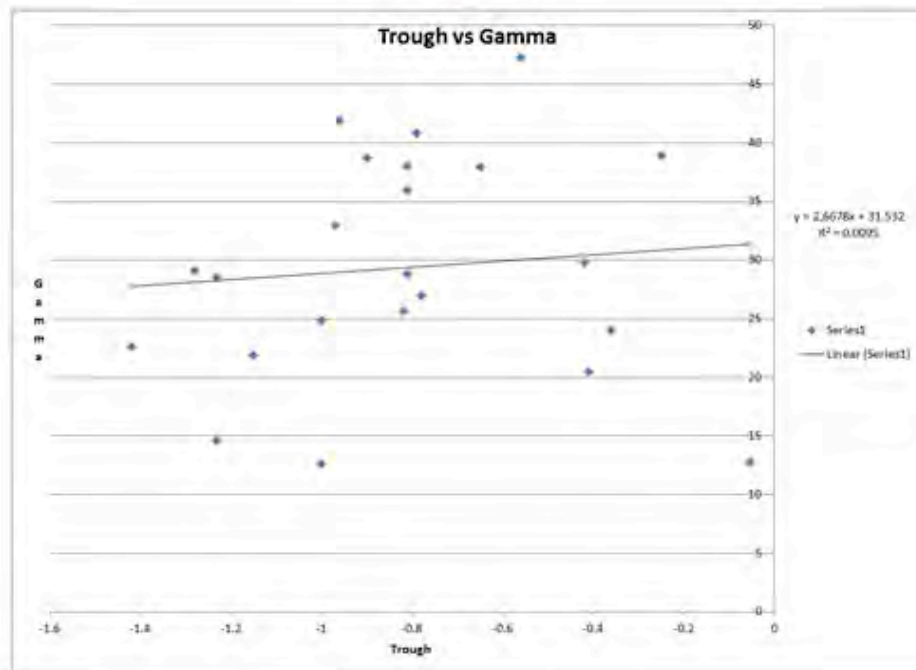


Figure 17: Trough vs Gamma

Peak vs porosity

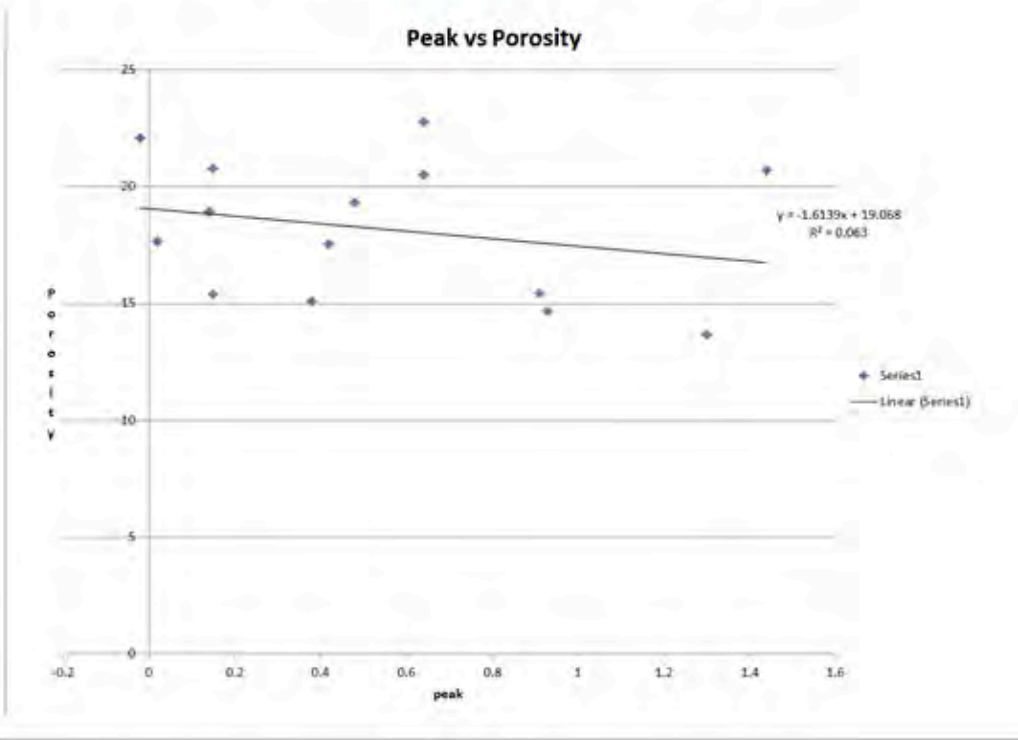


Figure 18: peak vs porosity cross-plot

Trough vs porosity

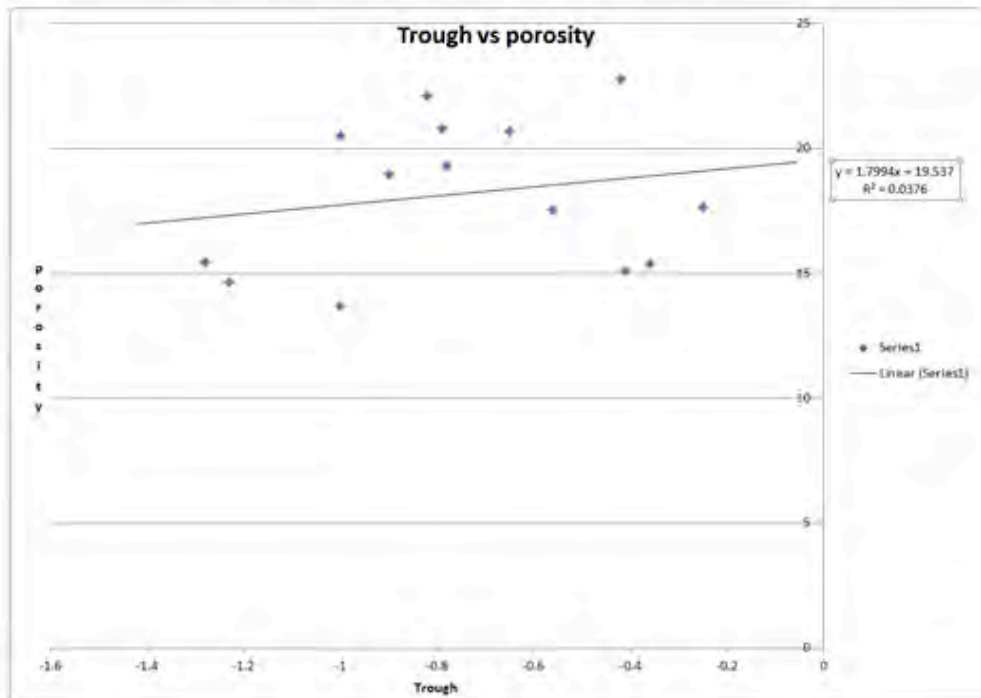


Figure 19: Trough vs Porosity